Electronic Supplementary Information (ESI)

Stable and Selective Electrosynthesis of Hydrogen Peroxide and the Electro-Fenton Process on $CoSe_2$ Polymorph Catalysts

Hongyuan Sheng,‡[a] Aurora N. Janes,‡[a] R. Dominic Ross,[a] Dave Kaiman,[a] Jinzhen Huang,[a,b] Bo Song,[a,b] J. R. Schmidt,*[a] and Song Jin*[a]

[a] Department of Chemistry, University of Wisconsin−Madison, 1101 University Avenue, Madison, Wisconsin 53706, United States

[b] Center for Composite Materials and Structures, Harbin Institute of Technology, Harbin 150001, China

‡ These authors contributed equally.

Corresponding Author

* E-mail: schmidt@chem.wisc.edu (J.R.S.); jin@chem.wisc.edu (S.J.)

Supplementary Experimental Section

Detailed Methods for Materials Synthesis. To synthesize cobalt hydroxide carbonate hydrate (CHCH) precursor, 1.275 mmol of $CoCl_2 \cdot 6H_2O$ (Sigma-Aldrich, 98.0%) and 3 mmol of urea (Riedel-de Haën, 99.5–100.5%) were dissolved in 75 mL of nanopure water and was heated at 120 °C for 5 h in a sealed 100-mL Teflon-lined stainless steel autoclave. The CHCH precursor was washed with water and ethanol and dried in vacuum at room temperature. The hydrothermal selenization of CHCH precursor was performed as follows: 4.29 g of NaOH (Sigma-Aldrich, ≥97.0%) and 571 mg of Se powder (Sigma-Aldrich, ≥99.5%) was mixed in 50 mL of nanopure water via sonication and was heated at 220 °C for 24 h in a sealed 80-mL autoclave; upon cooling to room temperature, 50 mg of CHCH precursor was suspended in 10 mL of nanopure water and added dropwise into the Se-containing solution under vigorous stirring, and then heated at 220 °C for another 24 h in the same autoclave. The as-converted $CoSe_2$ sample was washed with water and ethanol and dried in vacuum at room temperature. To control the polymorphism while removing the elemental Se impurity, an alumina boat containing 60 mg of as-converted $CoSe_2$ sample was placed in the center of a fused silica tube within a tube furnace (Thermo Scientific, TF55035A-1) and was annealed under a steady flow of Ar gas (99.999%) at 790 torr and 25 sccm. The *o*-$CoSe_2$ catalyst was obtained by annealing at 300 °C for 3 h, while the *c*-$CoSe_2$ catalyst was obtained by annealing at 500 °C for 1 h, both of which are polymorphic pure and free of elemental Se impurity. The *c*-CoS_2 catalyst was prepared via vapor-phase sulfidation: 50 mg of CHCH precursor was placed in an alumina boat at the center of the tube furnace, 2 g of sulfur (Sigma-Aldrich, 99.5–100.5%) was placed in another alumina boat at the farthest upstream position within the tube furnace, the sulfidation took place at 500 °C for 1 h. To synthesize CHCH nanowires on CFP substrate (CHCH/CFP), Teflon-coated carbon fiber paper (Fuel Cell Earth, TGP-H-060) was first treated with oxygen plasma at 150 W power for 5 min for each side and annealed in air at 700 °C for 5 min. A 3 cm × 6 cm piece of annealed CFP substrate was placed in the solution made of 2.1 mmol of $Co(NO_3)_2 \cdot 6H_2O$ (Sigma-Aldrich, ≥98.0%), 4.2 mmol of NH_4F (Sigma-Aldrich, ≥98.0%), and 10.5 mmol of urea in 80 mL of nanopure water and was heated in a sealed 100-mL autoclave at 110 °C for 5 h. The CHCH/CFP was sonicated in nanopure water to remove loosely-bound CHCH particles and dried under N_2 gas flow. *o*-$CoSe_2$/CFP and *c*-CoS_2/CFP were prepared via the same selenization or sulfidation method mentioned above, except for replacing CHCH

precursor with 1.5 cm × 6 cm pieces of CHCH/CFP. The as-converted *c*-CoS_2/CFP was immersed in CS_2 to remove any excess sulfur. All catalyst samples were stored in an Ar-filled glove box to minimize the exposure to air.

Detailed Sample Preparation for Materials Characterization. Scanning electron microscopy (SEM) samples were prepared by drop-casting catalysts in ethanol suspensions onto silicon wafers. Graphite substrates were used for X-ray photoelectron spectroscopy (XPS) experiments, which were made by cutting thin slices of graphite rod (Graphite Store, low wear EDM rod), abrading with 600 grit silicon carbide paper (Allied High Tech Products), and sonicating in nanopure water and ethanol until clean. The tested catalysts after rotating ring-disk electrode (RRDE) measurements were recovered from the disk electrode by sonicating in nanopure water and ultracentrifuging at 13.2K rpm for 1 min, followed by re-dispersing in minimal amount of nanopure water and drop-casting onto graphite substrates. XPS samples were used for Raman experiments without modification. X-ray absorption spectroscopy (XAS) samples were prepared by spreading a uniform layer of catalyst powders onto scotch tape, followed by folding into four layers to achieve a proper absorption length.

Supplementary Figures and Tables

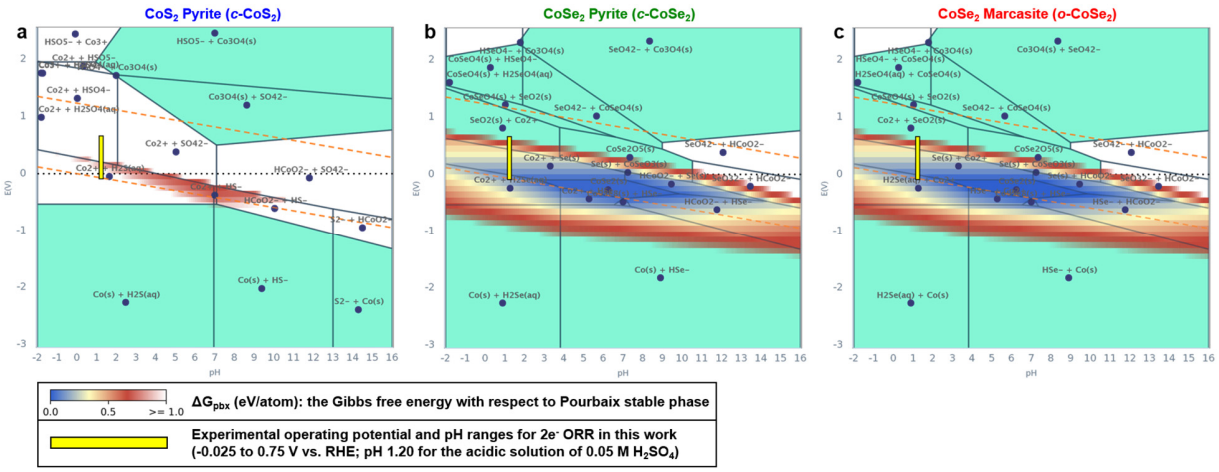

Fig. S1 Calculated bulk Pourbaix diagrams of (a) *c*-CoS_2, (b) *c*-$CoSe_2$, and (c) *o*-$CoSe_2$ assuming an ionic concentration of 10^{-6} mol/kg for each element of interest (59 ppb Co, 32 ppb S, and 79 ppb Se, which are reasonably low concentrations that can fairly reflect the acidic electrolyte solution of 0.05 M H_2SO_4 used in our experiments). These diagrams are adapted from the Materials Project.[S1] The diagram of *c*-CoS_2 is in agreement with that in a previous report.[S2] The multicolor gradient indicates the Gibbs free energy of the compound at a given set of potential and pH conditions with respect to its Pourbaix stable phase (ΔG_{pbx}), reflecting the electrochemical stability window of the compound. It was surmised in a previous report that materials with ΔG_{pbx} up to high values as much as 0.5 eV/atom can persist in electrochemical environments because of the energy barriers for the dissociation reactions.[S3] The electrochemical stability windows of both *c*-$CoSe_2$ (Fig. S1b) and *o*-$CoSe_2$ (Fig. S1c) are clearly much wider than that of *c*-CoS_2 (Fig. S1a) and, more importantly, cover the entire potential range of interest for $2e^-$ ORR in acidic solution (indicated by the yellow color bars).

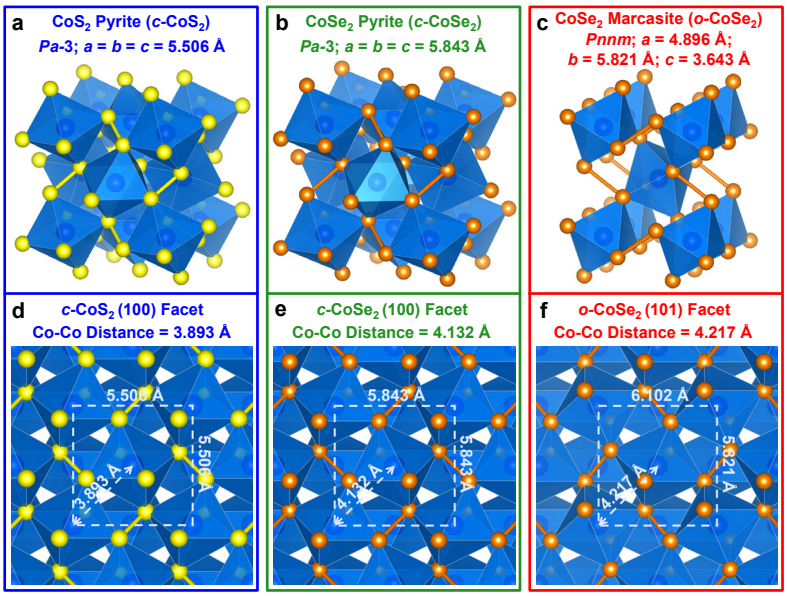

Fig. S2 Crystal structures, space groups, and lattice parameters of (a) *c*-CoS_2, (b) *c*-$CoSe_2$, and (c) *o*-$CoSe_2$. The Co, S, and Se atoms are displayed in blue, yellow, and orange, respectively. Top views and Co-Co interatomic distances of (d) *c*-CoS_2 (100), (e) *c*-$CoSe_2$ (100), and (f) *o*-$CoSe_2$ (101) surfaces. The *o*-$CoSe_2$ (101) surface mostly resembles the (100) surface of *c*-$CoSe_2$.

Table S1 Surface energies of the most thermodynamically stable facets of (a) cubic *c*-CoS_2 and *c*-$CoSe_2$, and (b) orthorhombic *o*-$CoSe_2$.

(a)

Facet	Surface Energy (eV/Å^2)	
	c-CoS_2 [a]	*c*-$CoSe_2$ [b]
(100)	0.032	0.044
(110)	0.060	0.064
(111)	0.057	0.069

(b)

Facet	Surface Energy (eV/Å^2)
	o-$CoSe_2$ [b]
(101)	0.044
(001)	0.060
(111)	0.060
(100)	0.070

[a] Data of *c*-CoS_2 are taken from ref. S4 and are calculated without a dispersion correction.

[b] Data of *c*-$CoSe_2$ and *o*-$CoSe_2$ are calculated with a dispersion correction using Grimme's D3(ABC) method.[S5]

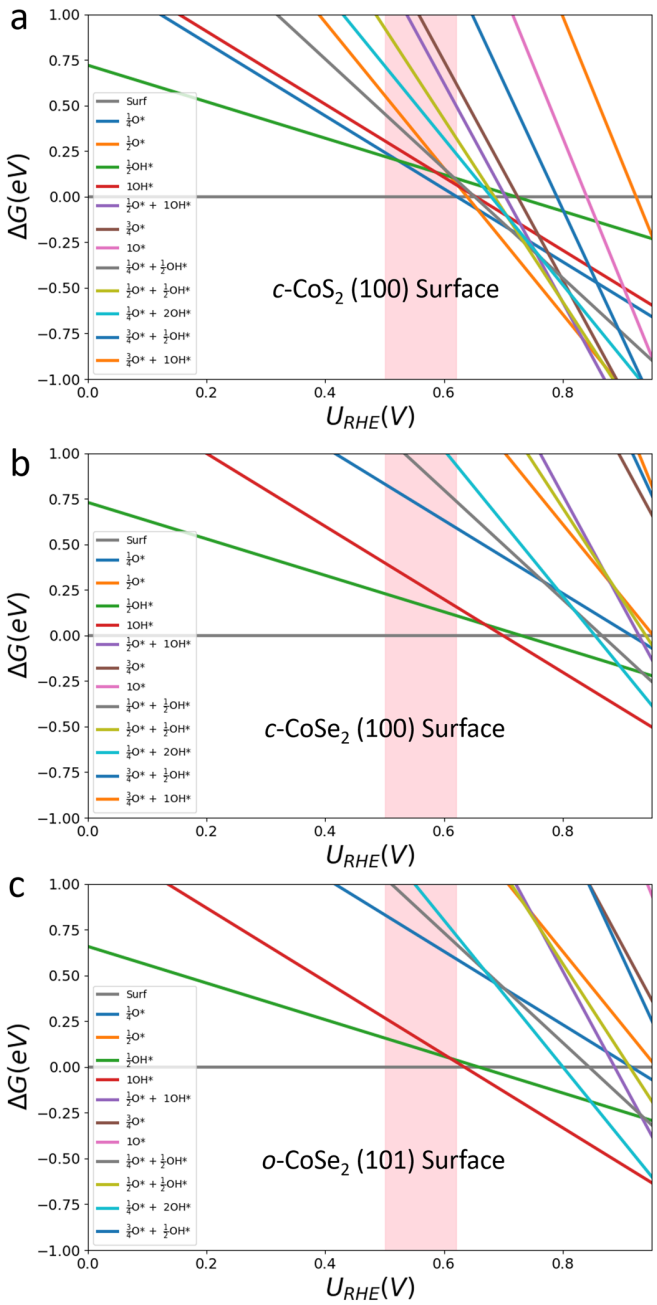

Fig. S3 Surface Pourbaix diagrams (ΔG vs. U_{RHE}) of (a) *c*-CoS_2 (100), (b) *c*-$CoSe_2$ (100), and (c) *o*-$CoSe_2$ (101) surfaces showing all the modeled surface coverages (from clean surface to ¾ ML O* + 1 ML OH*). The highlight regions in light red represent the experimental relevant potential range where the optimal H_2O_2 production performances are achieved. In comparison, Fig. 1 in the main text shows only the most stable surface coverages in the potential range of 0 to 1 V.

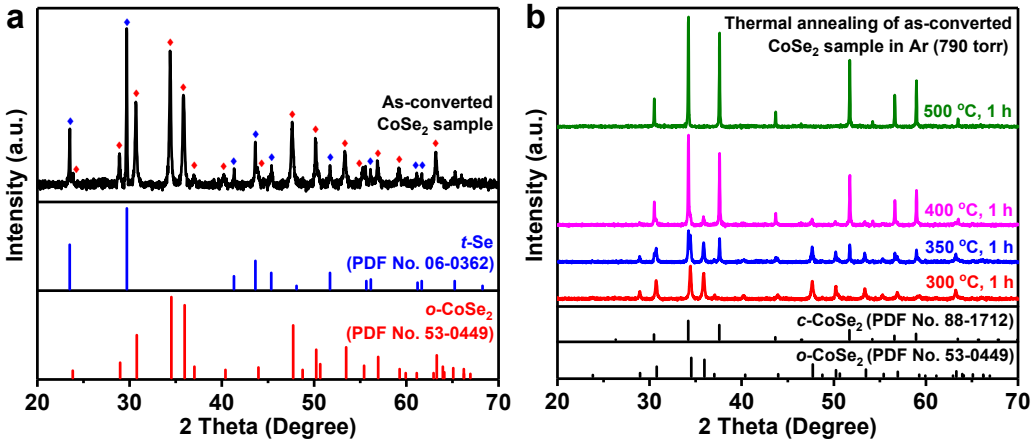

Fig. S4 (a) PXRD pattern of as-converted $CoSe_2$ sample, showing the coexistence of $CoSe_2$ marcasite with the orthorhombic phase (denoted as *o*-$CoSe_2$) and crystalline elemental Se impurity with the trigonal crystal structure (denoted as *t*-Se). (b) PXRD patterns of as-converted $CoSe_2$ sample annealed in Ar atmosphere (790 torr) at 300, 350, 400, and 500 °C for 1 h. Standard PXRD patterns of *o*-$CoSe_2$ (PDF No. 53-0449), *c*-$CoSe_2$ (PDF No. 88-1712), and *t*-Se (PDF No. 06-0362) are adapted from the International Centre for Diffraction Data (ICDD) database.

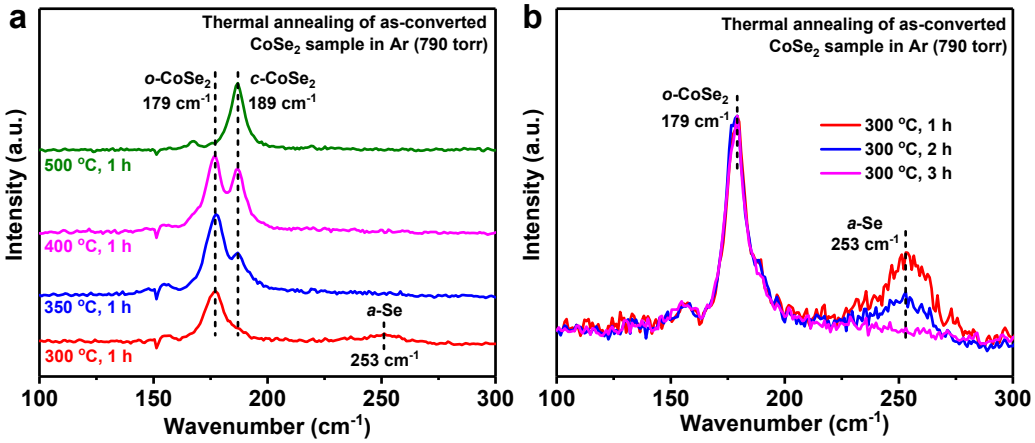

Fig. S5 (a) Raman spectra of as-converted $CoSe_2$ sample annealed in Ar atmosphere (790 torr) at 300, 350, 400, and 500 °C for 1 h, confirming the polymorphic transformation from *o*-$CoSe_2$ to *c*-$CoSe_2$. The weak signal at 253 cm^{-1}, only present in the *o*-$CoSe_2$ sample annealed at 300 °C for 1 h, corresponds to the residual amorphous elemental Se impurity (denoted as *a*-Se) due to the relatively low annealing temperature and short annealing time. (b) Raman spectra of as-converted $CoSe_2$ sample annealed in Ar atmosphere (790 torr) at 300 °C for 1, 2, and 3 h, showing that the residual *a*-Se impurity in the *o*-$CoSe_2$ sample can be completely removed by extending the annealing time without affecting the marcasite structure.

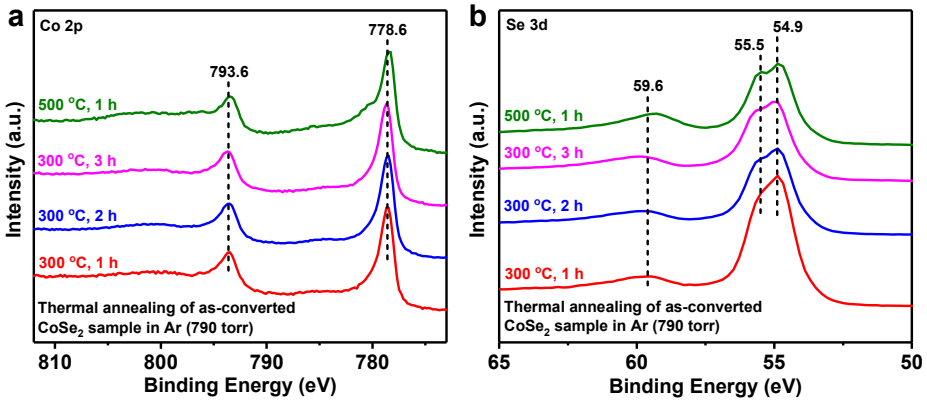

c

Annealing Condition	*Surface* Atomic Ratio of Co : Se
300 °C, 1 h	0.16
300 °C, 2 h	0.22
300 °C, 3 h	0.30
500 °C, 1 h	0.32

Fig. S6 (a) Co 2p and (b) Se 3d XPS spectra of as-converted $CoSe_2$ sample annealed in Ar atmosphere (790 torr) under different conditions (at 300 °C for 1, 2, and 3 h; at 500 °C for 1 h). The Co 2p signals (778.6 and 793.6 eV) suggest the +2 oxidation state of Co, meanwhile the weak Se 3d signals (59.6 eV) indicate the presence of small amounts of surface SeO_x. (c) Surface atomic ratio of Co : Se in as-converted $CoSe_2$ sample annealed under different conditions. The *o*-$CoSe_2$ sample annealed at 300 °C for 3 h exhibit almost the same surface atomic ratio as the *c*-$CoSe_2$ sample annealed at 500 °C for 1 h, showing that the amorphous elemental Se impurity in the *o*-$CoSe_2$ sample can be completely removed by extending the annealing time.

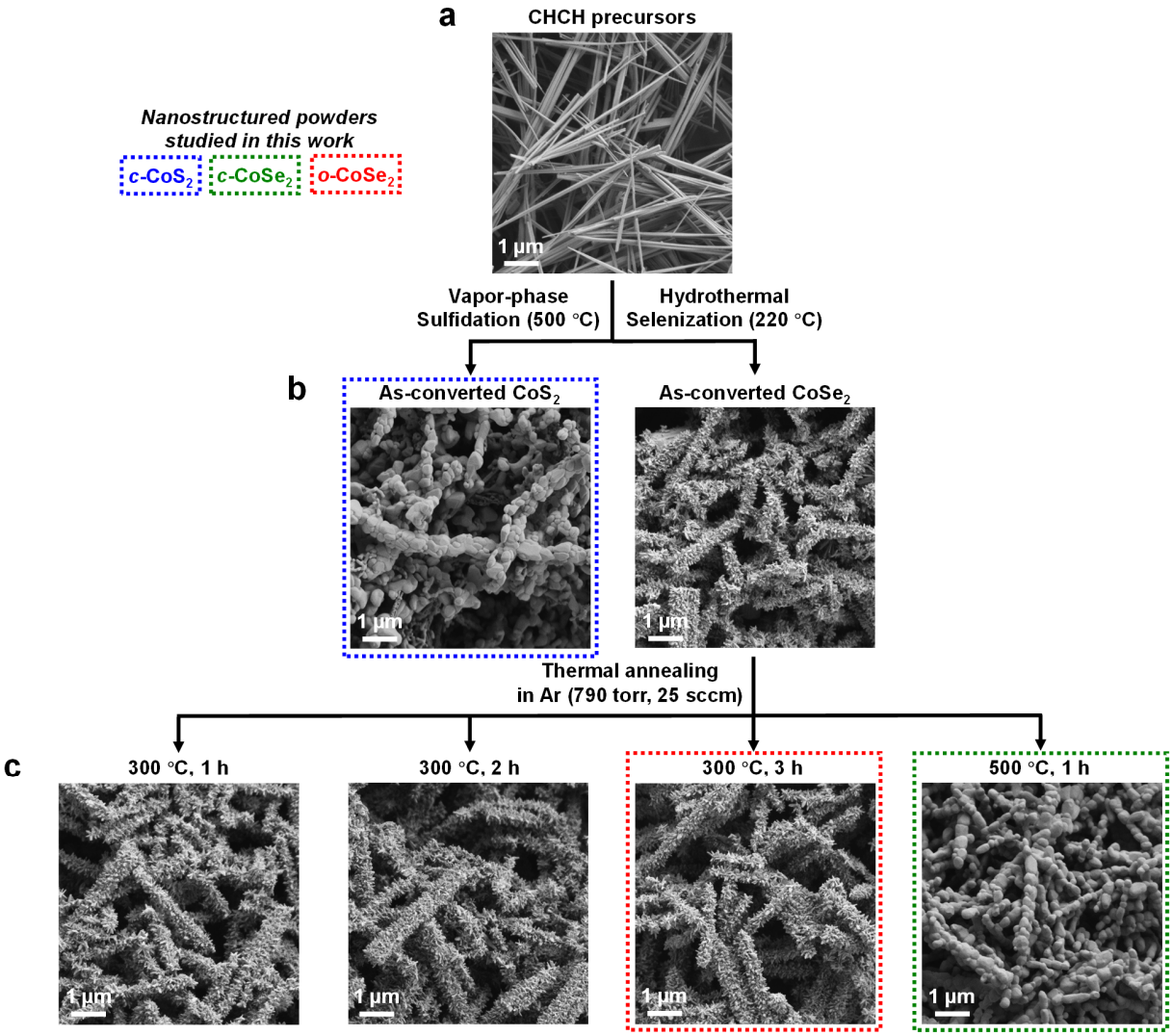

Fig. S7 SEM images of (a) CHCH precursor, (b) as-converted CoS_2 and $CoSe_2$ samples, and (c) as-converted $CoSe_2$ samples annealed in Ar atmosphere (790 torr) under different conditions (at 300 °C for 1, 2, and 3 h; at 500 °C for 1 h). Dashed color boxes specify the catalyst samples studied in this work: "*c*-CoS_2 catalyst" refers to as-converted CoS_2 sample; "*c*-$CoSe_2$ catalyst" refers to the *c*-$CoSe_2$ sample annealed at 500 °C for 1 h; "*o*-$CoSe_2$ catalyst" refers to the *o*-$CoSe_2$ sample annealed at 300 °C for 3 h.

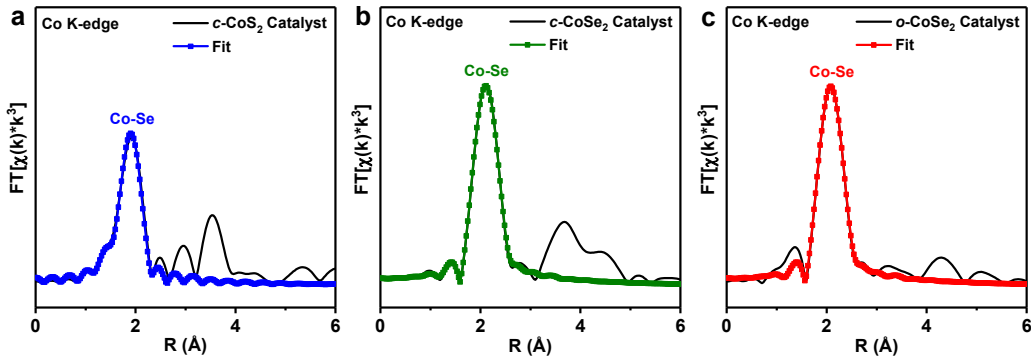

Fig. S8 The first shell fittings of Co K-edge EXAFS spectra of (a) *c*-CoS_2, (b) *c*-$CoSe_2$, and (c) *o*-$CoSe_2$ catalysts. The Fourier transform parameters and fitting results are summarized in Table S2.

Table S2 The first shell fitting results of Co K-edge EXAFS spectra of *c*-CoS_2, *c*-$CoSe_2$, and *o*-$CoSe_2$ catalysts.

Sample	Shell	N [c]	R (Å) [c]	σ^2 (10^{-3} Å^2) [c]	ΔE_0 (eV) [c]	Reduced χ^2 [c]	R-factor [c]
c-CoS_2 catalyst [a]	Co-S	5.8 ± 1.0	2.322 ± 0.005	5.8 ± 0.6	4.1 ± 0.9	73.8604902	0.0038897
c-$CoSe_2$ catalyst [b]	Co-Se	5.9 ± 0.9	2.425 ± 0.002	5.6 ± 0.3	1.3 ± 0.6	19.2082886	0.0016189
o-$CoSe_2$ catalyst [b]	Co-Se	5.9 ± 1.1	2.404 ± 0.005	5.7 ± 0.6	0.6 ± 1.4	62.3247933	0.0082318

[a] For *c*-CoS_2 catalyst, the Fourier transform parameters are: Hanning window, k_{min} = 3, k_{max} = 12, dk = 1, no phase correction; the fitting parameters are: r_{min} = 1, r_{max} = 2.3, dr = 0, fitting k-weight = 3.

[b] For *c*-$CoSe_2$ and *o*-$CoSe_2$ catalysts, the Fourier transform parameters are: Hanning window, k_{min} = 3, k_{max} = 12, dk = 1, no phase correction; the fitting parameters are: r_{min} = 1, r_{max} = 3, dr = 0, fitting k-weight = 3.

[c] N is the coordination number of the absorbing Co atom. R is the interatomic distance between the absorbing Co atom and the backscattering S/Se atom. σ^2 is the mean square relative displacement (i.e., the Debye-Waller factor). ΔE_0 is the energy shift parameter used to align the theoretical calculated spectrum to the energy grid of the measured spectrum. For all the first shell fittings, the amplitude reduction factor (S_0^2) is constrained to 0.90 as a reasonable estimation, and the added uncertainty in the coordination number (N) due to the estimation of S_0^2 has already been considered.[S6] Reduced χ^2 and R-factor are goodness-of-fit parameters.

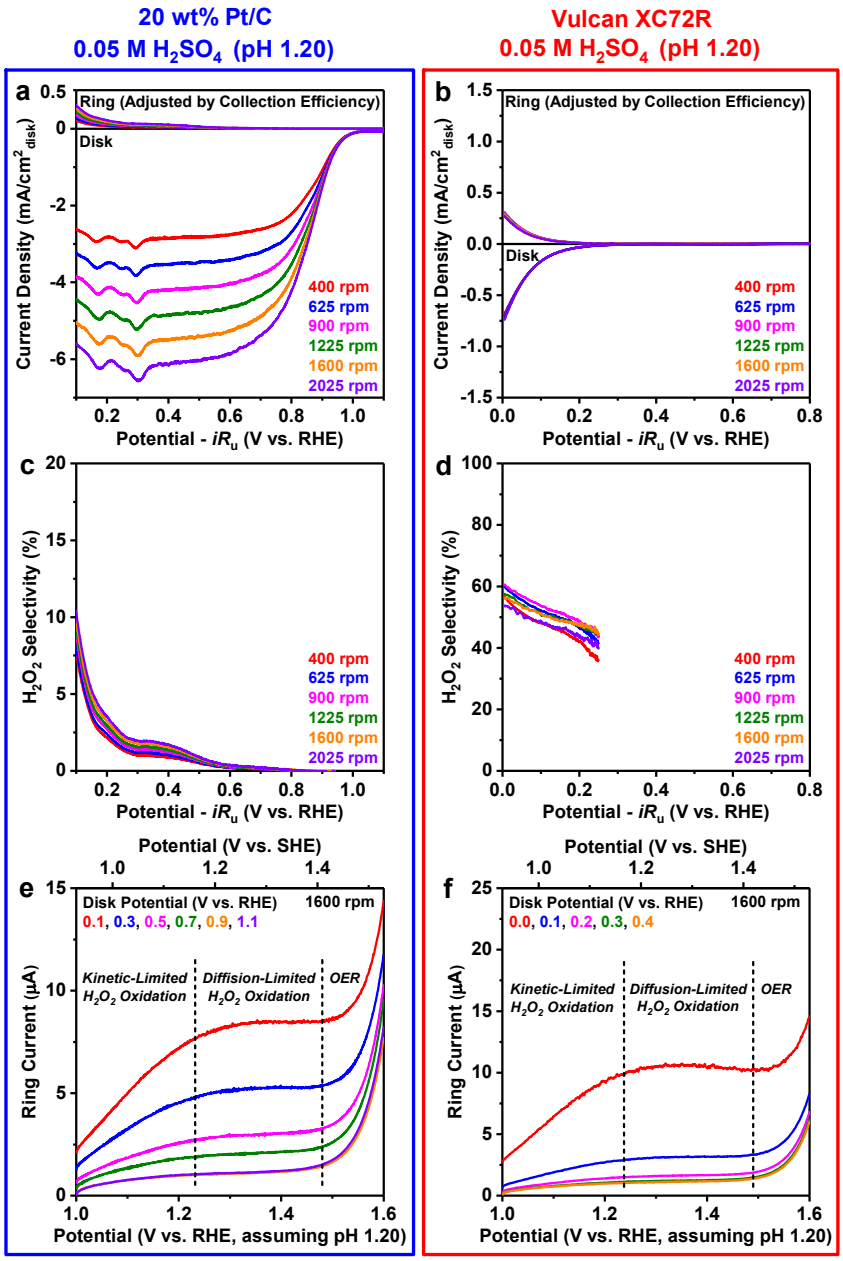

Fig. S9 RRDE voltammograms recorded at various rotation rates and the corresponding H_2O_2 selectivity of commercial (a,c) Pt/C and (b,d) carbon black catalysts in O_2-saturated 0.05 M H_2SO_4 solution (pH 1.20). The ring potential is set at 1.3 V vs. RHE, assuming the local pH near the electrode is equal to the pH of the bulk solution. (e,f) Linear sweep voltammograms of the ring electrode from 1.0 to 1.6 V vs. RHE recorded at the time when the catalyst-coated disk electrode is held at various constant potentials (either ORR-active or -inactive) at 1600 rpm in O_2-saturated 0.05 M H_2SO_4 solution (pH 1.20). *See additional discussion on page S12.*

Additional Discussion of Fig. S9 We reason that oxygen evolution reaction (OER) on the Pt ring electrode can serve as a probe reaction to monitor the local pH change, as the OER catalytic onset potential should not shift on the standard hydrogen electrode (SHE) scale if the local pH stays constant. We held the catalyst-coated disk electrode at various constant potentials (either ORR-active or -inactive), and performed linear sweep voltammetry (LSV) on the ring electrode to drive the kinetic- and diffusion-limited H_2O_2 oxidation (if any) and then OER as the ring potential was increased. As a result, the OER catalytic onset potential on the ring electrode remained the same whether or not ORR took place on these benchmark catalysts (Fig. S9e,f), confirming that the local pH was unaffected during electrochemical operations.

Table S3 Preparation of drop-casted *c*-$CoSe_2$, *o*-$CoSe_2$, and *c*-CoS_2 catalysts with various catalyst loadings for RRDE measurements in O_2-saturated 0.05 M H_2SO_4 solution (pH 1.20).

Catalyst	Catalyst Mass (mg)	5 wt% Nafion Volume (μL)	Water Volume (μL)	Drop-casted Volume (μL)	Catalyst loading ($\mu g_{Co}/cm^2_{disk}$)	Nafion Loading ($\mu g/cm^2_{disk}$)
c-CoS_2 catalyst	2.5	125	1125	10	76	348
	2.6	65	585	10	152	348
	2.7	45	405	10	229	348
	4.0	50	450	10	305	348
c-$CoSe_2$ catalyst	4.7	134	1202	10	76	348
	4.8	68	614	10	152	348
	4.5	42	383	10	229	348
	4.5	32	288	10	305	348
o-$CoSe_2$ catalyst	4.6	523	4704	10	19	348
	4.1	233	2096	10	38	348
	4.1	116	1048	10	76	348
	4.3	61	549	10	152	348

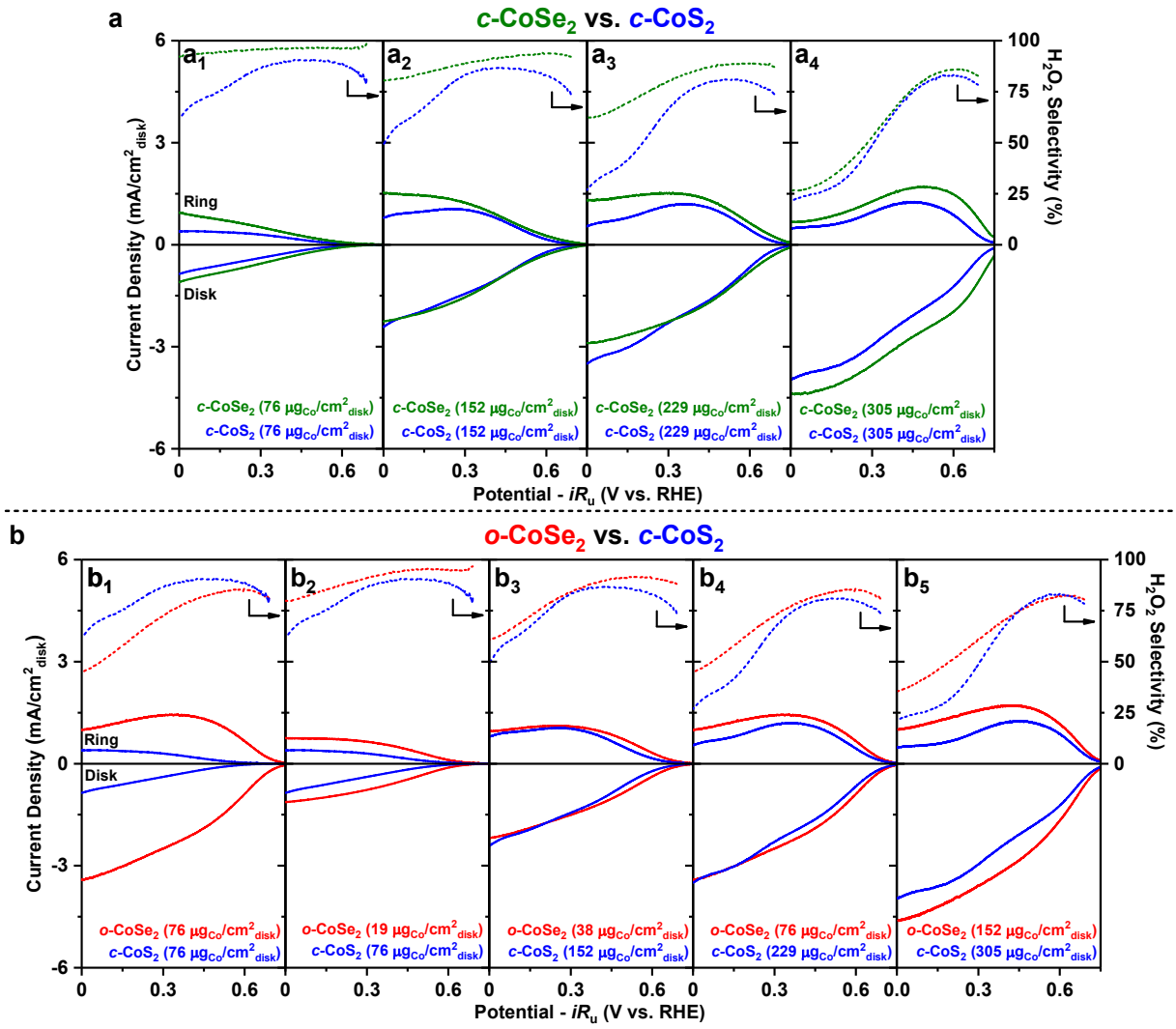

Fig. S10 (a) Comparisons of RRDE voltammograms recorded at 2025 rpm and the corresponding H_2O_2 selectivity of *c*-$CoSe_2$ and *c*-CoS_2 catalysts with the same catalyst loading (76, 152, 229, or 305 $\mu g_{Co}/cm^2_{disk}$) in O_2-saturated 0.05 M H_2SO_4 solution (pH 1.20). (b) Comparisons of RRDE voltammograms recorded at 2025 rpm and the corresponding H_2O_2 selectivity of *o*-$CoSe_2$ and *c*-CoS_2 catalysts (b_1) with the same catalyst loading (76 $\mu g_{Co}/cm^2_{disk}$) or (b_2–b_5) with different catalyst loadings that deliver similar overall ORR current densities (19, 38, 76, or 152 $\mu g_{Co}/cm^2_{disk}$ for *o*-$CoSe_2$; 76, 152, 229, or 305 $\mu g_{Co}/cm^2_{disk}$ for *c*-CoS_2) in O_2-saturated 0.05 M H_2SO_4 solution (pH 1.20).

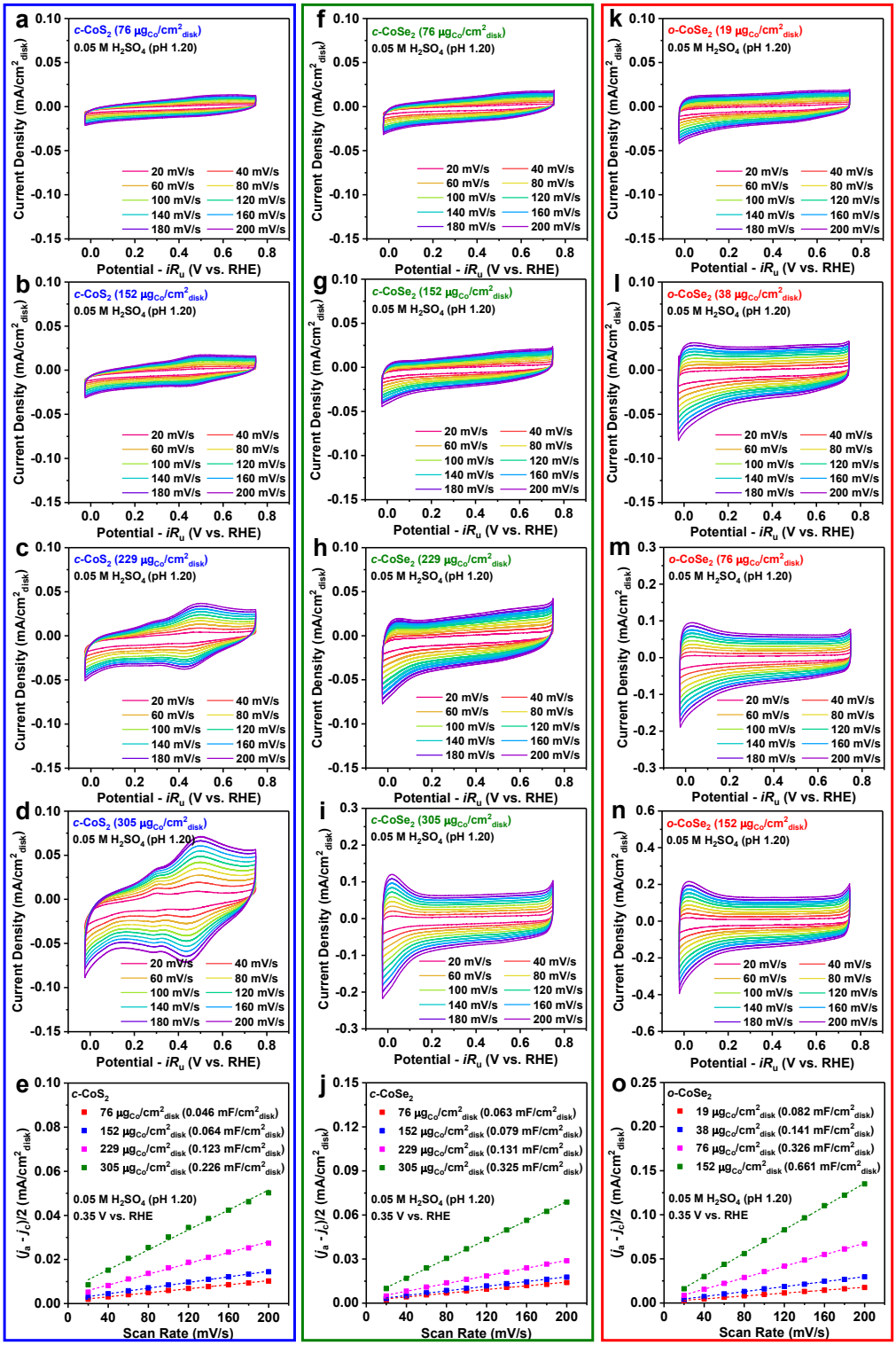

Fig. S11 C_{dl} measurements of (a–e) *c*-CoS_2, (f–j) *c*-$CoSe_2$, and (k–o) *o*-$CoSe_2$ catalysts with various catalyst loadings in the Ar-saturated 0.05 M H_2SO_4 solution (pH 1.20). *c*-CoS_2 displays redox features centered around 0.45 V vs. RHE, whereas both *c*-$CoSe_2$ and *o*-$CoSe_2$ polymorphs are free

of redox features over a wide potential window. Therefore, to minimize the interference from the redox features of *c*-CoS_2, we chose the fixed potential of 0.35 V vs. RHE to extract the C_{dl} values of all three catalysts from linear fittings, which are summarized in Table S4.

Table S4 Summary of the C_{dl} values (extracted from linear fittings at 0.35 V vs. RHE) of *c*-CoS_2, *c*-$CoSe_2$, and *o*-$CoSe_2$ catalysts with various catalyst loadings in the Ar-saturated 0.05 M H_2SO_4 solution (pH 1.20).

Catalyst	Catalyst loading ($\mu g_{Co}/cm^2_{disk}$)	C_{dl} at 0.35 V vs. RHE (mF/cm^2_{disk})
c-CoS_2 catalyst	76	0.046
	152	0.064
	229	0.123
	305	0.226
c-$CoSe_2$ catalyst	76	0.063
	152	0.079
	229	0.131
	305	0.325
o-$CoSe_2$ catalyst	19	0.082
	38	0.141
	76	0.326
	152	0.661

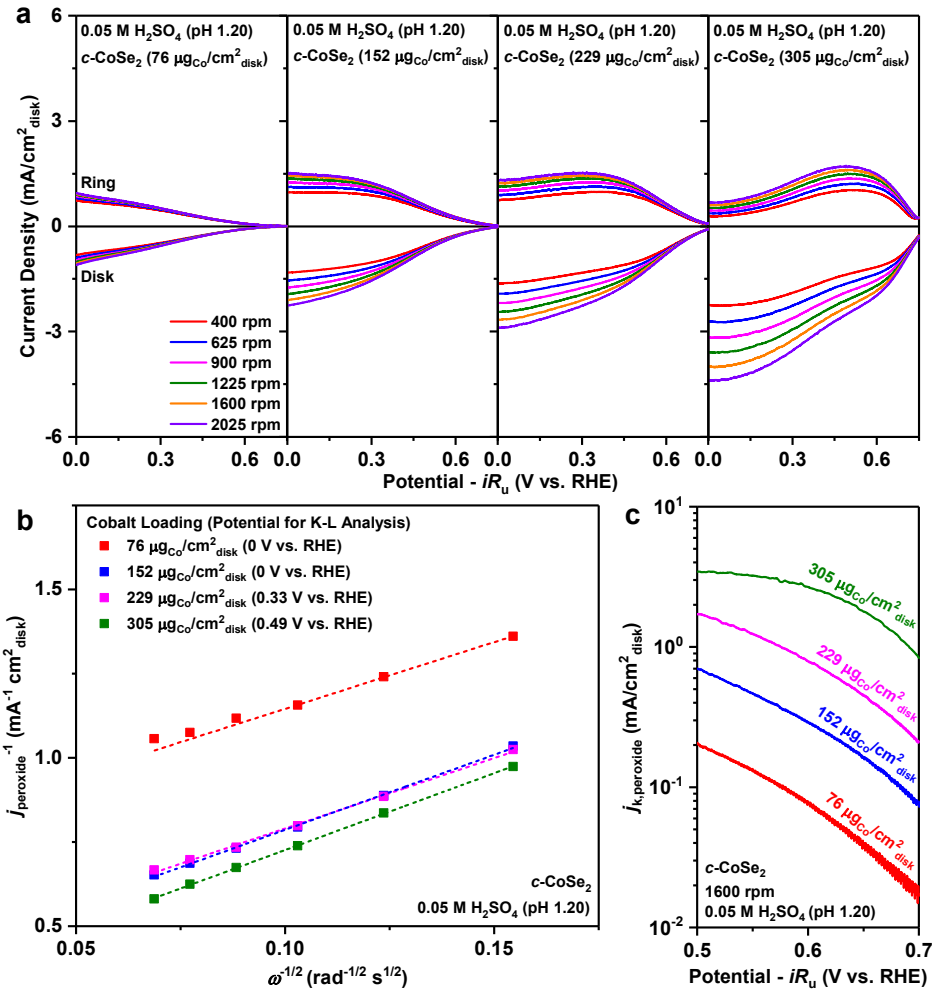

Fig. S12 (a) RRDE voltammograms of *c*-$CoSe_2$ catalyst with various catalyst loadings in O_2-saturated 0.05 M H_2SO_4 solution (pH 1.20) recorded at various rotation rates. (b) K-L analysis ($j_{peroxide}^{-1}$ vs. $\omega^{-1/2}$) based on RRDE measurements. (c) Kinetic current density for H_2O_2 production normalized to the geometric area of the disk electrode ($j_{k,peroxide}$) at 1600 rpm.

Table S5 K-L analysis ($j_{peroxide}^{-1}$ vs. $\omega^{-1/2}$) based on RRDE voltammograms of *c*-$CoSe_2$ catalyst with various catalyst loadings in O_2-saturated 0.05 M H_2SO_4 solution (pH 1.20) recorded at various rotation rates.

Catalyst loading ($\mu g_{Co}/cm^2_{disk}$)	Potential for K-L Analysis (V vs. RHE) [a]	Slope of $j_{peroxide}^{-1}$ vs. $\omega^{-1/2}$ ($mA^{-1}\ cm^2_{disk}\ rad^{1/2}\ s^{-1/2}$) [b]	$j_{L,peroxide}$ at 1600 rpm (mA/cm^2_{disk}) [c]
76	0	3.97	3.26
152	0	4.46	2.90
229	0.32	4.19	3.09
305	0.49	4.57	2.83

[a] For each catalyst loading, K-L analysis was performed at the potential where the approximate maximum of $j_{peroxide}$ was achieved.

[b] $j_{peroxide}^{-1} = j_{k,peroxide}^{-1} + j_{L,peroxide}^{-1} = j_{k,peroxide}^{-1} + B \times \omega^{-1/2}$, where $j_{peroxide}$ is the partial current density for H_2O_2 production (mA/cm^2_{disk}), $j_{k,peroxide}$ is the kinetic current density for H_2O_2 production (mA/cm^2_{disk}), $j_{k,peroxide}$ is the diffusion-limited current density for H_2O_2 production (mA/cm^2_{disk}), B is the slope ($mA^{-1}\ cm^2_{disk}\ rad^{1/2}\ s^{-1/2}$) of the linear fit of $j_{peroxide}^{-1}$ vs. $\omega^{-1/2}$ (see Fig. S12b).

[c] $j_{L,peroxide}$ at 1600 rpm $= B^{-1} \times \omega^{1/2} = B^{-1}$ ($mA\ cm^{-2}_{disk}\ rad^{-1/2}\ s^{1/2}$) $\times (1600 \times \pi / 30)^{1/2}$. The calculated $j_{L,peroxide}$ at 1600 rpm were in good agreement with the theoretical limiting current density for $2e^-$ ORR (~3 mA/cm^2_{disk} at 1600 rpm under O_2 saturation). Therefore, we used $j_{L,peroxide}$ = 3 mA/cm^2_{disk} in the equation $j_{k,peroxide} = \frac{j_{peroxide} \times j_{L,peroxide}}{j_{L,peroxide} - j_{peroxide}} = \frac{j_{peroxide} \times 3\ mA/cm^2_{disk}}{3\ mA/cm^2_{disk} - j_{peroxide}}$ to correct for mass-transport loss in $j_{peroxide}$.

Table S6 Summary of RRDE electrode information of *c*-$CoSe_2$ and *o*-$CoSe_2$ catalysts compared with *c*-CoS_2 and other reported $2e^-$ ORR electrocatalysts in *acidic* solution.

Classification	Catalyst	*Acidic* Electrolyte	Catalyst Loading	Reference
Earth-abundant transition metal compounds	*c*-$CoSe_2$	0.05 M H_2SO_4	305 $\mu g_{Co}/cm^2_{disk}$	this work
	o-$CoSe_2$	0.05 M H_2SO_4	152 $\mu g_{Co}/cm^2_{disk}$	this work
	c-CoS_2	0.05 M H_2SO_4	305 $\mu g_{Co}/cm^2_{disk}$	this work
Noble metal nanoparticles (NPs)	Pt-Hg NPs/C	0.1 M $HClO_4$	14 $\mu g_{Pt}/cm^2_{disk}$	ref. S7
	Pd-Hg NPs/C	0.1 M $HClO_4$	10 $\mu g_{Pd}/cm^2_{disk}$	ref. S8
	Pd-Au NPs	0.1 M $HClO_4$	10 $\mu g_{metal}/cm^2_{disk}$	ref. S9
Noble metal polycrystalline surfaces (pc)	Pt-Hg (pc)	0.1 M $HClO_4$	N/A	ref. S7
	Pd-Hg (pc)	0.1 M $HClO_4$	N/A	ref. S8
	Ag (pc)	0.1 M $HClO_4$	N/A	ref. S8
	Ag-Hg (pc)	0.1 M $HClO_4$	N/A	ref. S8
	Cu-Hg (pc)	0.1 M $HClO_4$	N/A	ref. S8
Noble metal single-atom catalysts	Pt_1/SC	0.1 M $HClO_4$	50 $\mu g_{catalyst}/cm^2_{disk}$ (5.0 wt% Pt)	ref. S10
	Pt_1/TiN	0.1 M $HClO_4$	15 $\mu g_{catalyst}$ (0.35 wt% Pt)	ref. S11
	h-Pt_1-CuS_x	0.1 M $HClO_4$	101 $\mu g_{catalyst}/cm^2_{disk}$ (24.8 at% Pt)	ref. S12
Transition metal single-atom catalysts	Co_1-N-C(1)	0.5 M H_2SO_4	100 $\mu g_{catalyst}/cm^2_{disk}$ (0.4 at% Co)	ref. S13
	Co_1-N-C(2)	0.1 M $HClO_4$	25 $\mu g_{catalyst}/cm^2_{disk}$ (1.4 wt% Co)	ref. S14
	Co_1-NG(O)	0.1 M $HClO_4$	10 $\mu g_{catalyst}/cm^2_{disk}$ (1.4 wt% Co)	ref. S15
	Mo_1-OSG-H	0.05 M H_2SO_4	101 $\mu g_{catalyst}/cm^2_{disk}$ (13.47 wt% Mo)	ref. S16
Carbon materials	O-CNTs	0.1 M $HClO_4$	101 $\mu g_{catalyst}/cm^2_{disk}$	ref. S17
	meso-BMP	0.1 M $HClO_4$	306 $\mu g_{catalyst}/cm^2_{disk}$	ref. S18
	NCMK	0.5 M H_2SO_4	50 $\mu g_{catalyst}/cm^2_{disk}$	ref. S19

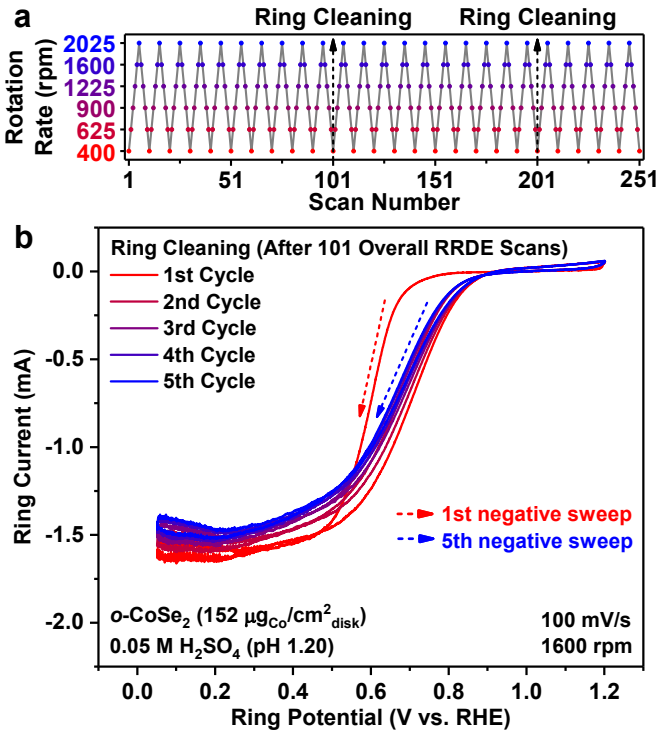

Fig. S13 (a) Rotation rate profile of catalyst stability tests from RRDE measurements in O_2-saturated 0.05 M H_2SO_4 solution (pH 1.20). (b) Electrochemical cleaning of the Pt ring electrode by running cyclic voltammetry at low overpotentials until observing typical ORR polarization curves for fresh Pt. The example shown here was performed during catalyst stability test of *o*-$CoSe_2$ (152 $\mu g_{Co}/cm^2_{disk}$) after 101 overall RRDE scans. In the first negative sweep, the ORR catalytic onset on the Pt ring electrode took place at a high overpotential. Starting the second negative sweep, the surface PtO_x was reduced and the ORR catalytic activity of the Pt ring electrode was recovered.

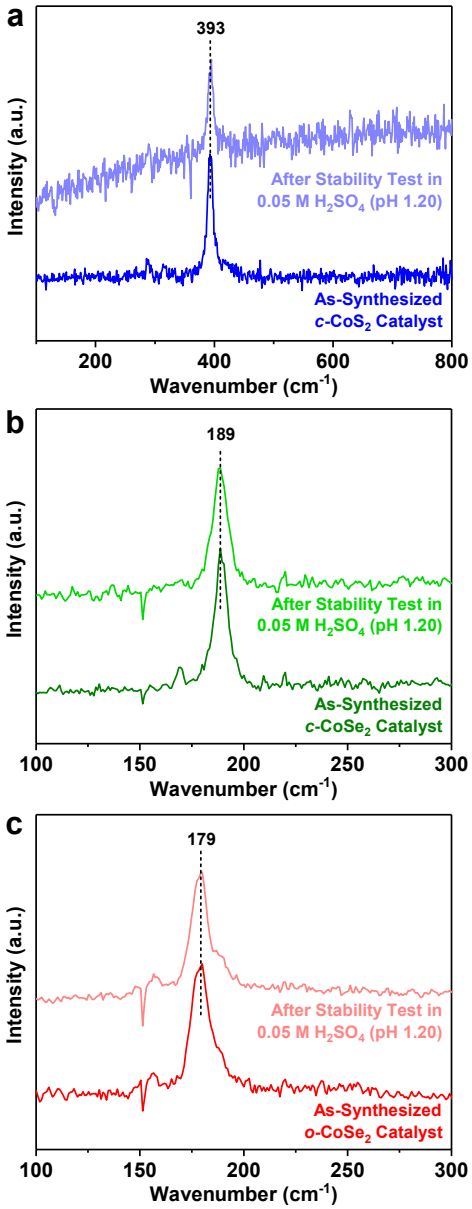

Fig. S14 Raman spectra of (a) *c*-CoS_2, (b) *c*-$CoSe_2$, and (c) *o*-$CoSe_2$ catalysts before and after catalyst stability tests from RRDE measurements in 0.05 M H_2SO_4 solution (pH 1.20). Background Raman spectra of bare graphite disk substrate were subtracted from as-measured Raman spectra of *c*-CoS_2, *c*-$CoSe_2$, and *o*-$CoSe_2$ catalysts.

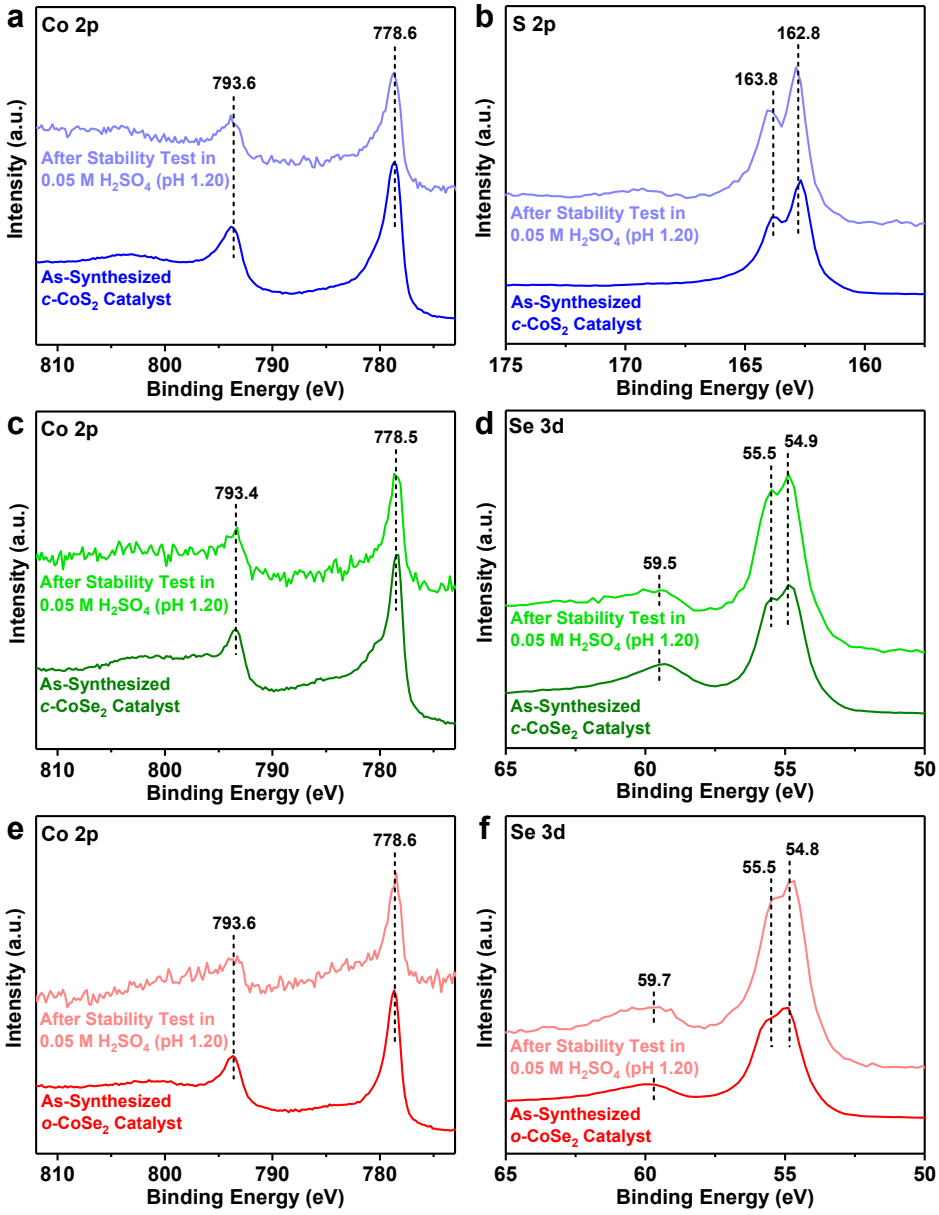

Fig. S15 XPS spectra of (a,b) *c*-CoS_2, (c,d) *c*-$CoSe_2$, and (e,f) *o*-$CoSe_2$ catalysts before and after catalyst stability tests from RRDE measurements in 0.05 M H_2SO_4 solution (pH 1.20). The strong Co 2p signals of all three catalysts (~778.6 and ~793.6 eV, see Fig. S15a,c,e) suggest the +2 oxidation state of Co. The strong S 2p signals of *c*-CoS_2 catalyst (162.8 and 163.8 eV, see Fig. S15b) correspond to the S_2^{2-} anions. The strong Se 3d signals of both $CoSe_2$ polymorphs (~54.9 and ~55.5 eV, see Fig. S15d,f) correspond to the Se_2^{2-} anions, whereas the weak Se 3d signals (~59.6 eV) indicate the presence of small amounts of surface SeO_x.

Table S7 Surface atomic ratios of Co : S/Se in *c*-CoS_2, *c*-$CoSe_2$, and *o*-$CoSe_2$ catalysts before and after catalyst stability tests from RRDE measurements (see XPS spectra in Fig. S15) and those of Co : Se in the *o*-$CoSe_2$/CFP electrode #3 before and after the bulk electrolysis at 0.5 V vs. RHE in 0.05 M H_2SO_4 for 5 h (see XPS spectra in Fig. S23).

Sample	Surface Atomic Ratio of Co : S/Se	
	Before	After
c-CoS_2	0.378 ± 0.004 [a]	0.25 ± 0.03 [b]
c-$CoSe_2$	0.325 ± 0.001 [a]	0.25 ± 0.03 [b]
o-$CoSe_2$	0.29 ± 0.02 [a]	0.26 ± 0.04 [b]
o-$CoSe_2$/CFP #3	0.32 [c]	0.26 [c]

[a] The averages and standard deviations for the as-synthesized catalysts come from two samples made from two replicate synthesis. See representative XPS spectra in Fig. S15.

[b] The averages and standard deviations for the used catalysts come from four samples recovered from four replicate RRDE measurements. See representative XPS spectra in Fig. S15.

[c] See XPS spectra in Fig. S23.

Table S8 ICP-MS analysis of the tested electrolyte solutions after catalyst stability tests of *c*-CoS_2 (305 $\mu g_{Co}/cm^2_{disk}$), *c*-$CoSe_2$ (305 $\mu g_{Co}/cm^2_{disk}$), and *o*-$CoSe_2$ (152 $\mu g_{Co}/cm^2_{disk}$) from RRDE measurements in 0.05 M H_2SO_4 solution.

ICP-MS Sample		Intensity	Standard Curve	[Co]	Average Cobalt Leaching Rate
Standard solution of $CoSO_4$ in 0.05 M H_2SO_4	[Co] = 0 ug_{Co}/L	0.7	y = 42.9 x + 3.4 (r^2 = 0.99995)	-	-
	[Co] = 5.0 ug_{Co}/L	214.2		-	-
	[Co] = 20.0 ug_{Co}/L	872.3		-	-
	[Co] = 50.0 ug_{Co}/L	2146.6		-	-
Tested electrolyte solution of 0.05 M H_2SO_4 (45 mL)	*c*-CoS_2 (305 $\mu g_{Co}/cm^2_{disk}$) [a] 2.5 h (151 RRDE scans)	1576.0	-	36.6 ug_{Co}/L	0.66 ug_{Co}/h
	c-$CoSe_2$ (305 $\mu g_{Co}/cm^2_{disk}$) [a] 2.5 h (151 RRDE scans)	941.6	-	21.8 ug_{Co}/L	0.39 ug_{Co}/h
	o-$CoSe_2$ (152 $\mu g_{Co}/cm^2_{disk}$) [a] 4.2 h (251 RRDE scans)	1228.7	-	28.5 ug_{Co}/L	0.31 ug_{Co}/h

[a] Geometric area of the disk electrode is 0.126 cm^2_{disk}.

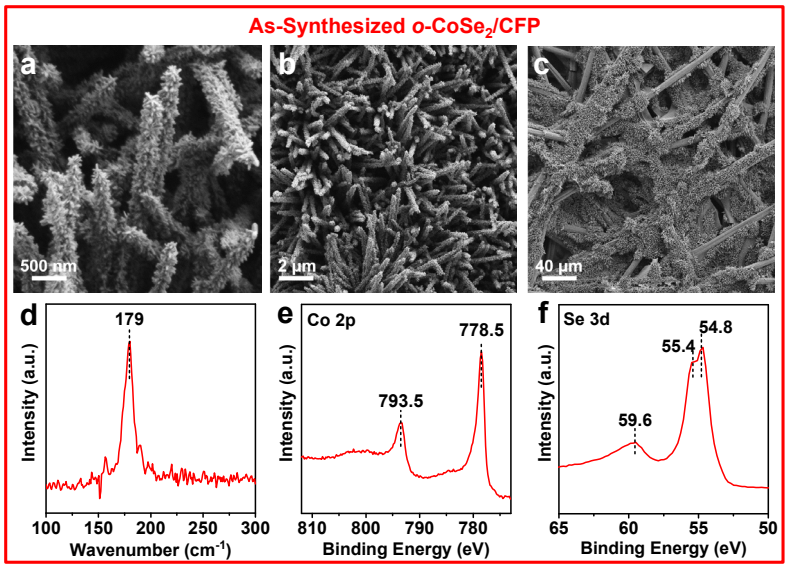

Fig. S16 (a–c) SEM images at different magnifications, (d) Raman spectra, (e) Co 2p and (f) Se 3d XPS spectra of as-synthesized *o*-$CoSe_2$/CFP. Background Raman spectra of bare carbon fiber paper substrate were subtracted from as-measured Raman spectra of *o*-$CoSe_2$/CFP.

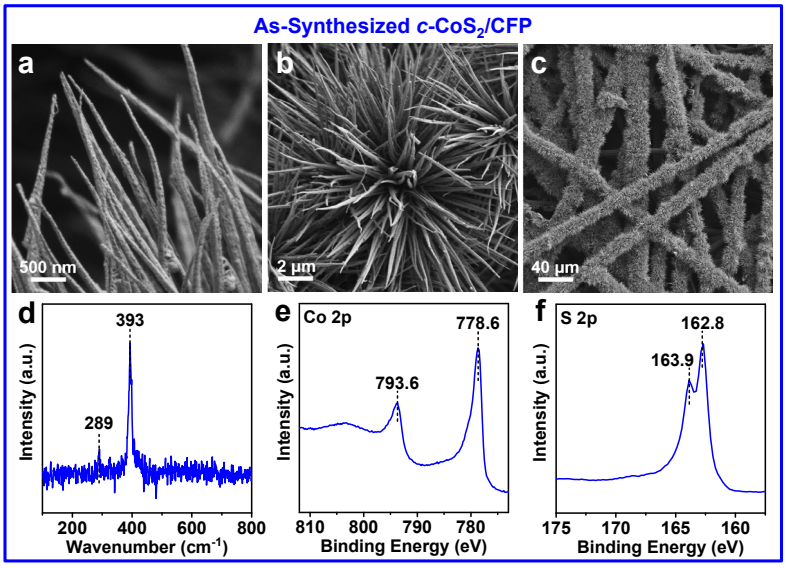

Fig. S17 (a–c) SEM images at different magnifications, (d) Raman spectra, (e) Co 2p and (f) S 2p XPS spectra of as-synthesized *c*-CoS_2/CFP. Background Raman spectra of bare carbon fiber paper substrate were subtracted from as-measured Raman spectra of *c*-CoS_2/CFP.

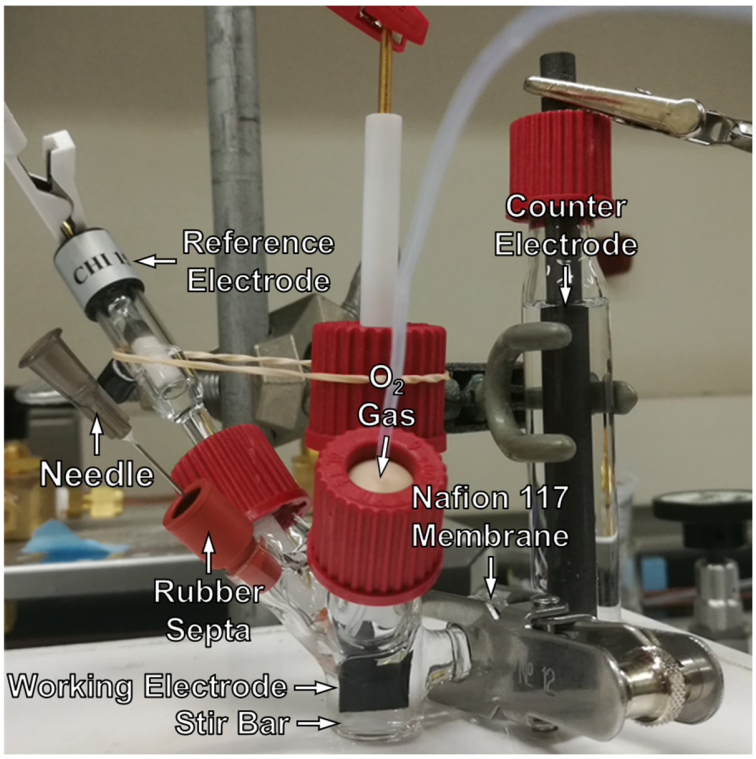

Fig. S18 Digital photograph of the two-compartment three-electrode H-cell setup used for bulk electrosynthesis of H_2O_2. Nafion 117 membrane was used to separate the two compartments to avoid the oxidation of H_2O_2 product on the counter electrode. A minimal volume (3–4 mL) of electrolyte solution was used and vigorously stirred at 1200 rpm in the working electrode compartment to achieve higher H_2O_2 concentrations under facilitated mass transfer of O_2 gas. A blanket of O_2 gas was maintained over the surface of O_2-saturated electrolyte solution during bulk electrosynthesis. A rubber septum punctured with a syringe needle served as the gas outlet, which was removed when a small aliquot of electrolyte solution was sampled from the working electrode compartment for chemical detection of H_2O_2 product and was capped for the rest of the time to minimize the evaporation of electrolyte solution during bulk electrosynthesis.

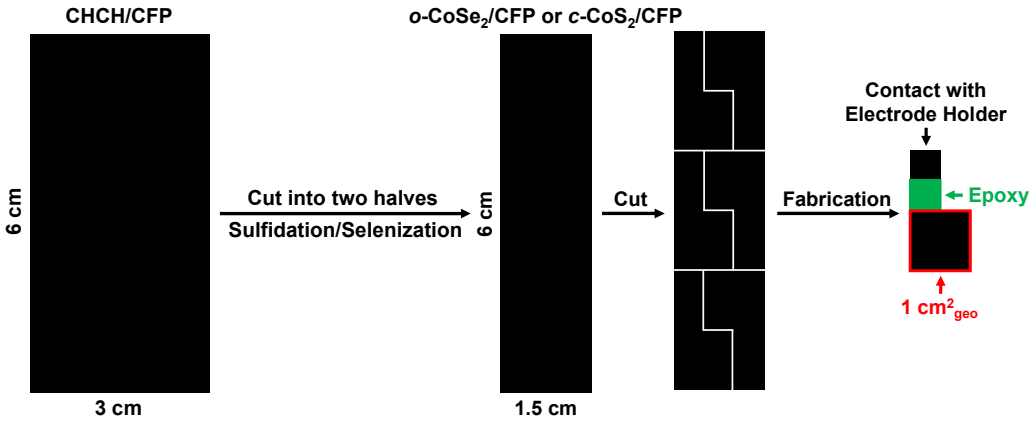

Fig. S19 Fabrication of *o*-$CoSe_2$/CFP and *c*-CoS_2/CFP working electrodes with the same geometric area of ~1 cm^2_{geo} for bulk electrosynthesis of H_2O_2.

Table S9 Summary of the catalyst loadings of *o*-$CoSe_2$/CFP and *c*-CoS_2/CFP working electrodes.

Sample	Mass (mg)	Catalyst loading ($\mu g_{Co}/cm^2_{geo}$)
Bare CFP (3 × 6 cm^2_{geo})	142.8	-
CHCH/CFP (3 × 6 cm^2_{geo})	155.4	~376 [a]
CHCH/CFP (1st half; 1.5 × 6 cm^2_{geo}) [b]	78.1	~376 [a]
o-$CoSe_2$/CFP (1st half; 1.5 × 6 cm^2_{geo}) [b]	84.5	~384
CHCH/CFP (2nd half; 1.5 × 6 cm^2_{geo}) [b]	76.7	~376 [a]
c-CoS_2/CFP (2nd half; 1.5 × 6 cm^2_{geo}) [b]	77.3	~363

[a] The chemical formula of CHCH is $Co(CO_3)_{0.5}(OH)\cdot 0.11H_2O$ (MW = 107.93 g/mol).

[b] The geometric area is illustrated in Fig. S19.

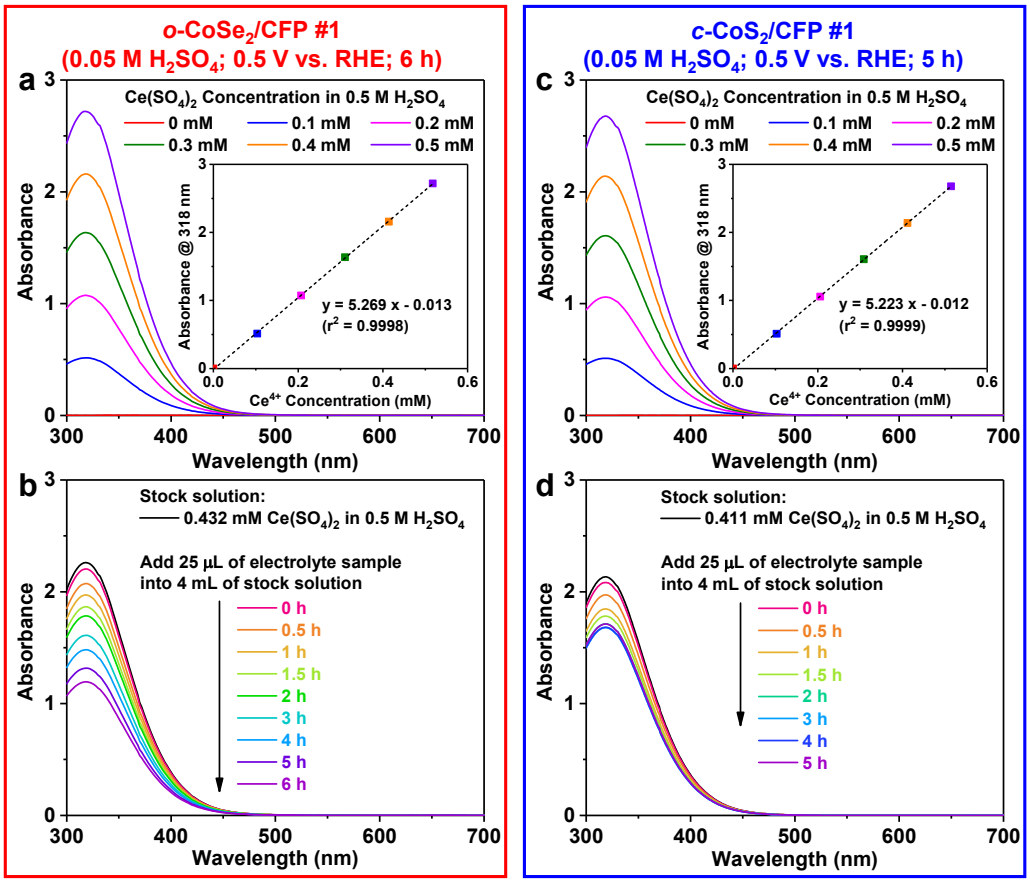

Fig. S20 (a,c) Absorption spectra of standard solutions of $Ce(SO_4)_2$ (up to 0.5 mM) in 0.5 M H_2SO_4 and the resultant calibration curve at the peak wavelength of 318 nm (shown as an inset) measured for each run of bulk electrolysis: (a) *o*-$CoSe_2$/CFP electrode #1 and (c) *c*-CoS_2/CFP electrode #1 (see Fig. 6 in the main text). (b,d) Absorption spectra of stock solution of $Ce(SO_4)_2$ (~0.4 mM, exact concentration was determined from the respective calibration curve) in 0.5 M H_2SO_4 with and without being titrated with a small aliquot of electrolyte solution sampled from the working electrode compartment at various time points during each run of bulk electrolysis: (b) *o*-$CoSe_2$/CFP electrode #1 and (d) *c*-CoS_2/CFP electrode #1 (see Fig. 6 in the main text).

Table S10 Summary of cumulative H_2O_2 concentration and cumulative H_2O_2 yield during the bulk electrolysis runs of *o*-$CoSe_2$/CFP electrode #1 and *c*-CoS_2/CFP electrode #1 at 0.5 V vs. RHE in 0.05 M H_2SO_4 solution (continuously operated for 5–6 h, see Fig. 6 in the main text).

Electrolyte Evaporation Rate During Bulk Electrolysis Run	Time Point for Aliquot Sampling	Electrolyte Volume Before (and After) Aliquot Sampling [b]	Absorbance at 318 nm Before (and After) Adding Aliquot into Ce^{4+} Stock Solution [c]	Ce^{4+} Concentration Before (and After) Adding Aliquot into Ce^{4+} Stock Solution	Cumulative H_2O_2 Concentration [f]	Cumulative H_2O_2 Yield (and H_2O_2 Produced Between Two Nearest Aliquot Samplings [g])
o-$CoSe_2$/CFP #1 (0.05 M H_2SO_4; 0.5 V vs. RHE; 6 h)	0 h	4 mL (3.975 mL)	2.262 (2.204)	0.432 (0.421) [d]	0.67 mM	0 μmol (0 μmol)
	0.5 h	3.840 mL (3.815 mL)	2.262 (2.074)	0.432 (0.396)	2.65 mM	7.53 μmol (7.53 μmol)
	1 h	3.679 mL (3.654 mL)	2.262 (1.972)	0.432 (0.377)	4.21 mM	12.91 μmol (5.38 μmol)
Initial Volume = 4 mL	1.5 h	3.519 mL (3.494 mL)	2.262 (1.866)	0.432 (0.357)	5.83 mM	18.04 μmol (5.13 μmol)
Final Volume = 2.15 mL [a]	2 h	3.358 mL (3.333 mL)	2.262 (1.785)	0.432 (0.341)	7.04 mM	21.31 μmol (3.27 μmol)
Aliquot Volume = 25 μL × 9	3 h	3.062 mL (3.037 mL)	2.262 (1.610)	0.432 (0.308)	9.71 mM	27.57 μmol (6.27 μmol)
Electrolyte Evaporation Rate $= \frac{(4\ \text{mL} - 25\mu\text{L} \times 9) - 2.15\ \text{mL}}{6\ \text{h}}$	4 h	2.767 mL (2.742 mL)	2.262 (1.481)	0.432 (0.284)	11.68 mM	30.39 μmol (2.82 μmol)
= 0.271 mL/h	5 h	2.471 mL (2.446 mL)	2.262 (1.317)	0.432 (0.252)	14.19 mM	33.44 μmol (3.05 μmol)
	6 h	2.175 mL (2.15 mL)	2.262 (1.195)	0.432 (0.229)	16.08 mM	33.69 μmol (0.25 μmol)
c-CoS_2/CFP #1 (0.05 M H_2SO_4; 0.5 V vs. RHE; 5 h)	0 h	4 mL (3.975 mL)	2.133 (2.083)	0.411 (0.401) [e]	0.57 mM	0 μmol (0 μmol)
	0.5 h	3.854 mL (3.829 mL)	2.133 (1.972)	0.411 (0.380)	2.28 mM	6.51 μmol (6.51 μmol)
Initial Volume = 4 mL	1 h	3.707 mL (3.682 mL)	2.133 (1.846)	0.411 (0.356)	4.22 mM	13.42 μmol (6.91 μmol)
Final Volume = 2.59 mL [a]	1.5 h	3.562 mL (3.537 mL)	2.133 (1.783)	0.411 (0.344)	5.20 mM	16.39 μmol (2.97 μmol)
Aliquot Volume = 25 μL × 8	2 h	3.416 mL (3.391 mL)	2.133 (1.713)	0.411 (0.330)	6.28 mM	19.45 μmol (3.06 μmol)
Electrolyte Evaporation Rate	3 h	3.149 mL (3.124 mL)	2.133 (1.678)	0.411 (0.324)	6.81 mM	19.61 μmol (0.16 μmol)
$= \frac{(4\ \text{mL} - 25\mu\text{L} \times 8) - 2.59\ \text{mL}}{5\ \text{h}}$	4 h	2.882 mL (2.857 mL)	2.133 (1.683)	0.411 (0.325)	6.74 mM	17.77 μmol (-1.84 μmol)
= 0.242 mL/h	5 h	2.615 mL (2.59 mL)	2.133 (1.712)	0.411 (0.330)	6.28 mM	14.94 μmol (-2.83 μmol)

[a] Final volume of electrolyte solution at the end of bulk electrolysis was determined by transferring all the remaining electrolyte solution out of the working compartment using an Eppendorf pipette.

[b] The volume of electrolyte solution before and after each aliquot sampling was calculated under the assumption that the electrolyte evaporation rate was constant throughout the bulk electrolysis.

[c] For chemical detection of H_2O_2 product, 25-μL aliquot of electrolyte solution was quantitatively added into 4 mL of Ce^{4+} stock solution (see Fig. S20b,d).

[d] For the bulk electrolysis run of *o*-$CoSe_2$/CFP #1, the calibration curve of absorbance at 318 nm vs. Ce^{4+} concentration (mM) was y = 5.269 x - 0.013 (see Fig. S20a).

[e] For the bulk electrolysis run of *o*-$CoSe_2$/CFP #1, the calibration curve of absorbance at 318 nm vs. Ce^{4+} concentration (mM) was y = 5.223 x - 0.012 (see Fig. S20c).

[f] Cumulative H_2O_2 Concentration (mM) = $(4\ \text{mL} \times [Ce^{4+}]_{before} - 4.025\ \text{mL} \times [Ce^{4+}]_{after}) / (2 \times 0.025\ \text{mL})$, where $[Ce^{4+}]_{before}$ and $[Ce^{4+}]_{after}$ are the Ce^{4+} concentration (mM) before and after adding 25-μL aliquot of electrolyte solution into 4 mL of Ce^{4+} stock solution, respectively. For example, for the bulk electrolysis run of *o*-$CoSe_2$/CFP #1, cumulative H_2O_2 concentration at 0.5 h = (4 mL × 0.432 mM – 4.025 mL × 0.396 mM) / (2 × 0.025 mL) = 2.65 mM.

[g] H_2O_2 produced between two nearest aliquot samplings (μmol) = $[H_2O_2]_{later} \times V_{later} - [H_2O_2]_{earlier} \times V_{earlier}$, where $[H_2O_2]_{later}$ and $[H_2O_2]_{earlier}$ are the cumulative H_2O_2 concentration (mM) at the later time point and at the earlier time point, respectively; V_{later} (mL) is the electrolyte volume at the later time point *before* aliquot sampling; $V_{earlier}$ (mL) is the electrolyte volume at the earlier time point *after* aliquot sampling. For example, for the bulk electrolysis run of *o*-$CoSe_2$/CFP #1, H_2O_2 produced between 0 h and 0.5 h = 2.65 mM × 3.840 mL – 0.67 mM × 3.975 mL = 7.53 μmol, H_2O_2 produced between 0.5 h and 1 h = 4.21 mM × 3.679 mL – 2.65 mM × 3.815 mL = 5.38 μmol.

Table S11 Summary of cumulative H_2O_2 selectivity and cumulative Faradaic efficiency during the bulk electrolysis runs of *o*-$CoSe_2$/CFP electrode #1 and *c*-CoS_2/CFP electrode #1 at 0.5 V vs. RHE in 0.05 M H_2SO_4 solution (continuously operated for 5–6 h, see Fig. 6 in the main text).

Bulk Electrolysis Run	Time Point for Aliquot Sampling	Cumulative H_2O_2 Yield (and H_2O_2 Produced Between Two Nearest Aliquot Samplings [a])	Cumulative Charge Passed	Theoretical H_2O_2 Yield [b]	Cumulative H_2O_2 Selectivity [c]	Cumulative Faradaic Efficiency [d]
	0 h	0 μmol (0 μmol)	0 C	0 μmol	-	-
	0.5 h	7.53 μmol (7.53 μmol)	2.013 C	10.43 μmol	83.8%	72.2%
	1 h	12.91 μmol (5.38 μmol)	3.520 C	18.24 μmol	82.9%	70.8%
	1.5 h	18.04 μmol (5.13 μmol)	4.875 C	25.26 μmol	83.3%	71.4%
***o*-$CoSe_2$/CFP #1 (0.05 M H_2SO_4; 0.5 V vs. RHE; 6 h)**	2 h	21.31 μmol (3.27 μmol)	6.053 C	31.37 μmol	80.9%	67.9%
	3 h	27.57 μmol (6.27 μmol)	8.045 C	41.69 μmol	79.6%	66.1%
	4 h	30.39 μmol (2.82 μmol)	9.642 C	49.96 μmol	75.6%	60.8%
	5 h	33.44 μmol (3.05 μmol)	10.98 C	56.87 μmol	74.1%	58.8%
	6 h	33.69 μmol (0.25 μmol)	12.15 C	62.95 μmol	69.7%	53.5%
	0 h	0 μmol (0 μmol)	0 C	0 μmol	-	-
	0.5 h	6.51 μmol (6.51 μmol)	2.905 C	15.05 μmol	60.4%	43.3%
	1 h	13.42 μmol (6.91 μmol)	6.144 C	31.84 μmol	59.3%	42.2%
	1.5 h	16.39 μmol (2.97 μmol)	9.729 C	50.42 μmol	49.1%	32.5%
***c*-CoS_2/CFP #1 (0.05 M H_2SO_4; 0.5 V vs. RHE; 5 h)**	2 h	19.45 μmol (3.06 μmol)	13.71 C	71.03 μmol	43.0%	27.4%
	3 h	19.61 μmol (0.16 μmol)	22.28 C	115.44 μmol	29.0%	17.0%
	4 h	17.77 μmol (-1.84 μmol)	31.26 C	161.97 μmol	19.8%	11.0%
	5 h	14.94 μmol (-2.83 μmol)	40.60 C	210.40 μmol	13.3%	7.1%

[a] See Table S10.

[b] Theoretical H_2O_2 Yield (μmol) = Cumulative Charge Passed (C) $\times \frac{1\ \text{mol e}^-}{96485\ \text{C}} \times \frac{1\ \text{mol H}_2\text{O}_2}{2\ \text{mol e}^-} \times \frac{10^6\ \mu\text{mol H}_2\text{O}_2}{1\ \text{mol H}_2\text{O}_2}$

[c] Cumulative H_2O_2 Selectivity (%) $= \frac{\text{Cumulative O}_2\text{ Consumption that Yields H}_2\text{O}_2\ (\mu\text{mol})}{\text{Cumulative O}_2\text{ Consumption}\ (\mu\text{mol})} \times 100\%$

$= \frac{\text{Cumulative H}_2\text{O}_2\text{ Yield}\ (\mu\text{mol})}{\text{Cumulative H}_2\text{O}_2\text{ Yield}\ (\mu\text{mol}) + \text{Cumulative O}_2\text{ Consumption that Yields H}_2\text{O}\ (\mu\text{mol})} \times 100\%$

$= \frac{\text{Cumulative H}_2\text{O}_2\text{ Yield}\ (\mu\text{mol})}{\text{Cumulative H}_2\text{O}_2\text{ Yield}\ (\mu\text{mol}) + [\ \text{Cumulative Charge Passed (C)} - \text{Cumulative H}_2\text{O}_2\text{ Yield}\ (\mu\text{mol}) \times \frac{1\ \text{mol H}_2\text{O}_2}{10^6\ \mu\text{mol H}_2\text{O}_2} \times \frac{1\ \text{mol O}_2}{1\ \text{mol H}_2\text{O}_2} \times \frac{2\ \text{mol e}^-}{1\ \text{mol O}_2} \times \frac{96485\ \text{C}}{1\ \text{mol e}^-}\ ] \times \frac{1\ \text{mol e}^-}{96485\ \text{C}} \times \frac{2\ \text{mol H}_2\text{O}}{4\ \text{mol e}^-} \times \frac{1\ \text{mol O}_2}{2\ \text{mol H}_2\text{O}} \times \frac{10^6\ \mu\text{mol O}_2}{1\ \text{mol O}_2}} \times 100\%$

[d] Cumulative Faradaic Efficiency (%) $= \frac{\text{Cumulative Charge Passed that Yields H}_2\text{O}_2\ (\text{C})}{\text{Cumulative Charge Passed (C)}} \times 100\%$

$= \frac{\text{Cumulative H}_2\text{O}_2\text{ Yield}\ (\mu\text{mol}) \times \frac{1\ \text{mol H}_2\text{O}_2}{10^6\ \mu\text{mol H}_2\text{O}_2} \times \frac{2\ \text{mol e}^-}{1\ \text{mol H}_2\text{O}_2} \times \frac{96485\ \text{C}}{1\ \text{mol e}^-}}{\text{Cumulative Charge Passed (C)}} \times 100\%$

Table S12 ICP-MS analysis of the tested electrolyte solutions of 0.05 M H_2SO_4 after the bulk electrolysis runs of *o*-$CoSe_2$/CFP electrode #1 and *c*-CoS_2/CFP electrode #1 (continuously operated for 5 h, see Fig. 6 in the main text) as well as *o*-$CoSe_2$/CFP electrode #2 and *c*-CoS_2/CFP electrode #2 (first operated for 1.5 h, and then operated for another 2.5 h after the H_2O_2-free electrolyte solution was reintroduced, see Fig. S21).

ICP-MS Sample		Intensity	Standard Curve	[Co] in Diluted ICP-MS Sample	Final Electrolyte Volume After Bulk Electrolysis	Average Cobalt Leaching Rate [b]
Standard solution of $CoSO_4$ in 0.05 M H_2SO_4	[Co] = 0 ug_{Co}/L	1.0	y = 45.5 x – 114.7 (r^2 = 0.99996)	-	-	-
	[Co] = 52.3 ug_{Co}/L	2058.4		-	-	-
	[Co] = 104.5 ug_{Co}/L	4715.2		-	-	-
	[Co] = 209.1 ug_{Co}/L	9469.0		-	-	-
	[Co] = 522.7 ug_{Co}/L	23605.7		-	-	-
	[Co] = 1045.5 ug_{Co}/L	47499.7		-	-	-
1:15 Dilution of tested electrolyte solution with 0.05 M H_2SO_4 [a]	***o*-$CoSe_2$/CFP #1** (4 mL of 0.05 M H_2SO_4; 0.5 V vs. RHE; **6 h**)	5720.2	-	128.2 ug_{Co}/L	2.15 mL	0.69 ug_{Co}/h
	***o*-$CoSe_2$/CFP #2** (3 mL of 0.05 M H_2SO_4; 0.5 V vs. RHE; **1.5 h**)	2724.3	-	62.4 ug_{Co}/L	2.00 mL	1.25 ug_{Co}/h
	***o*-$CoSe_2$/CFP #2 (Reused)** (3 mL of 0.05 M H_2SO_4; 0.5 V vs. RHE; **2.5 h**)	256.9	-	8.16 ug_{Co}/L	1.99 mL	0.10 ug_{Co}/h
	***c*-CoS_2/CFP #1** (4 mL of 0.05 M H_2SO_4; 0.5 V vs. RHE; **5 h**)	16299.7	-	360.6 ug_{Co}/L	2.59 mL	2.80 ug_{Co}/h
	***c*-CoS_2/CFP #2** (3 mL of 0.05 M H_2SO_4; 0.5 V vs. RHE; **1.5 h**)	4201.4	-	94.8 ug_{Co}/L	2.06 mL	1.97 ug_{Co}/h
	***c*-CoS_2/CFP #2 (Reused)** (3 mL of 0.05 M H_2SO_4; 0.5 V vs. RHE; **2.5 h**)	8400.3	-	187.1 ug_{Co}/L	2.08 mL	2.31 ug_{Co}/h

[a] To prepare ICP-MS sample, 1 part of tested electrolyte solution was diluted with 14 part of 0.05 M H_2SO_4.

[b] Average Cobalt Leaching Rate (μg_{Co}/h) = $\frac{\text{[Co] in Diluted ICP-MS Sample } (ug_{Co}/L) \times 15 \times \text{Final Electrolyte Volume After Bulk Electrolysis (mL)} \times \frac{1\ L}{10^3\ mL}}{\text{Bulk Electrolysis Time (h)}}$

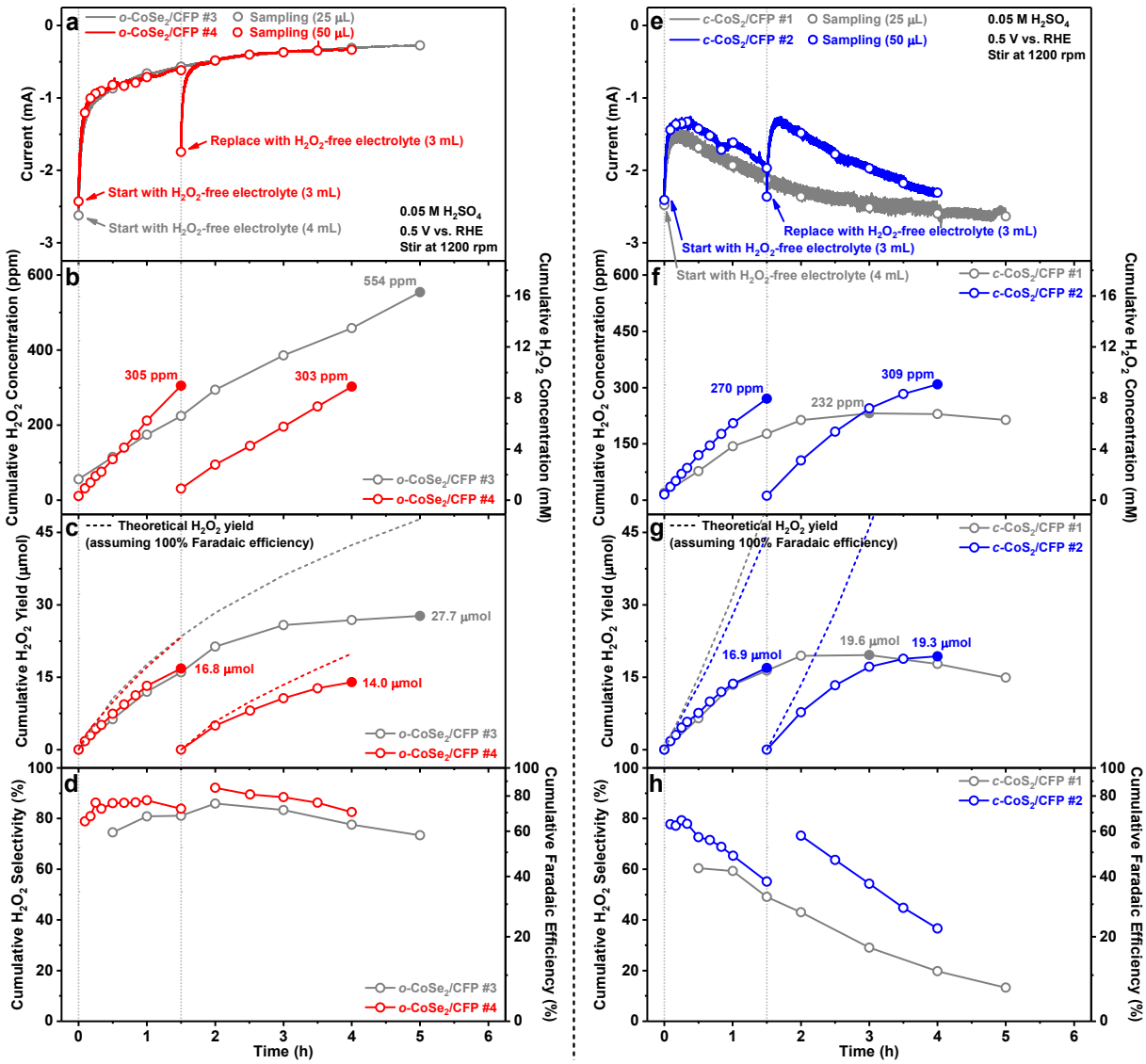

Fig. S21 (a) Chronoamperometry curves of *o*-$CoSe_2$/CFP electrode #3 (continuously operated for 5 h) and #4 (first operated for 1.5 h, and then operated for another 2.5 h after the H_2O_2-free electrolyte solution was reintroduced) at 0.5 V vs. RHE in O_2-saturated 0.05 M H_2SO_4 solution (pH 1.20) under vigorous stirring (1200 rpm). (b) Cumulative H_2O_2 concentration, (c) cumulative H_2O_2 yield, and (d) cumulative H_2O_2 selectivity and Faradaic efficiency during the bulk electrolysis runs of *o*-$CoSe_2$/CFP electrode #3 and #4. (e–h) Similar bulk experiments were performed on *c*-CoS_2/CFP electrode #1 (continuously operated for 5 h) and #2 (first operated for 1.5 h, and then operated for another 2.5 h after the H_2O_2-free electrolyte solution was reintroduced).

Table S13 ICP-MS analysis of the tested electrolyte solutions of 0.05 M H_2SO_4 after the bulk electrolysis runs of *o*-$CoSe_2$/CFP electrode #3 (continuously operated for 5 h, see Fig. S21) and #4 (first operated for 1.5 h, and then operated for another 2.5 h after the H_2O_2-free electrolyte solution was reintroduced, see Fig. S21).

ICP-MS Sample		Intensity	Standard Curve	[Co] in Diluted ICP-MS Sample	Final Electrolyte Volume After Bulk Electrolysis	Average Cobalt Leaching Rate [b]
Standard solution of $CoSO_4$ in 0.05 M H_2SO_4	[Co] = 0 ug_{Co}/L	0.9	y = 47.2 x + 25.6 (r^2 = 0.99996)	-	-	-
	[Co] = 100.0 ug_{Co}/L	4791.0		-	-	-
	[Co] = 200.0 ug_{Co}/L	9331.4		-	-	-
	[Co] = 500.0 ug_{Co}/L	23832.4		-	-	-
	[Co] = 1000.0 ug_{Co}/L	47176.3		-	-	-
1:15 Dilution of tested electrolyte solution with 0.05 M H_2SO_4 [a]	***o*-$CoSe_2$/CFP #3** (4 mL of 0.05 M H_2SO_4; 0.5 V vs. RHE; **5 h**)	2041.4	-	42.7 ug_{Co}/L	2.00 mL	0.26 ug_{Co}/h
	***o*-$CoSe_2$/CFP #4** (3 mL of 0.05 M H_2SO_4; 0.5 V vs. RHE; **1.5 h**)	4873.8	-	102.7 ug_{Co}/L	1.79 mL	1.84 ug_{Co}/h
	***o*-$CoSe_2$/CFP #4 (Reused)** (3 mL of 0.05 M H_2SO_4; 0.5 V vs. RHE; **2.5 h**)	830.7	-	17.1 ug_{Co}/L	1.71 mL	0.18 ug_{Co}/h

[a] To prepare ICP-MS sample, 1 part of tested electrolyte solution was diluted with 14 part of 0.05 M H_2SO_4.

[b] Average Cobalt Leaching Rate (μg_{Co}/h) = $\frac{\text{[Co] in Diluted ICP-MS Sample } (ug_{Co}/L) \times 15 \times \text{Final Electrolyte Volume After Bulk Electrolysis (mL)} \times \frac{1\ L}{10^3\ mL}}{\text{Bulk Electrolysis Time (h)}}$

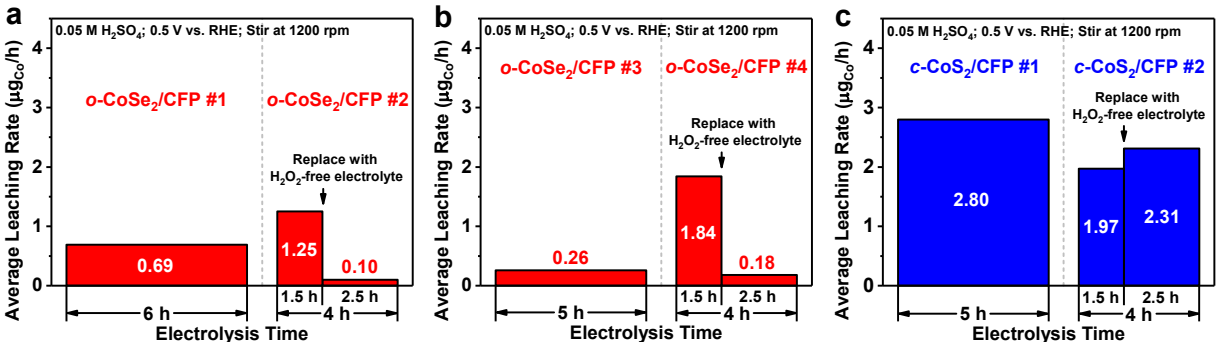

Fig. S22 ICP-MS analysis of the tested electrolyte solutions of 0.05 M H_2SO_4 after the bulk electrolysis runs of (a) *o*-$CoSe_2$/CFP electrode #1 and #2, (b) *o*-$CoSe_2$/CFP electrode #3 and #4, and (c) *c*-CoS_2/CFP electrode #1 and #2. The transient catalyst leaching of *o*-$CoSe_2$ took place mostly at the beginning of bulk electrolysis and was minimal afterwards (see Fig. S22a,b for two replicate experiments), whereas *c*-CoS_2 continuously leached into electrolyte solution throughout the entire bulk electrolysis (see Fig. S22c). *See additional discussion on page S33.*

Additional Discussion of Fig. S22 Based on the low steady state cobalt leaching rate of the *o*-$CoSe_2$ catalyst (0.10 and 0.18 μg_{Co}/h in two replicate experiments, see Fig. S22a,b) and the catalyst mass loading of the *o*-$CoSe_2$/CFP electrode (~370 μg_{Co} on each electrode with ~1 cm^2_{geo}, see Table S9), a back-of-the-envelope estimate suggests the *o*-$CoSe_2$ catalyst, in theory, could last for several months under the operating conditions of the bulk electrosynthesis of H_2O_2. An example calculation is shown below.

$$370\ \mu g_{Co}/cm^2_{geo} \times 1\ cm^2_{geo} \times \frac{1\ h}{0.10\ \mu g_{Co}} \times \frac{1\ day}{24\ h} \times \frac{1\ month}{30\ day} = 5.1\ months$$

Table S14 Comparisons of the leaching results of *o*-$CoSe_2$/CFP under operating conditions of the bulk electrosynthesis of H_2O_2 to those of other cobalt-based electrocatalysts reported for water splitting reactions, due to the fact that there has been no rigorous analysis of metal leaching in the recently reported earth-abundant $2e^-$ ORR catalysts.

Reaction [1]	Electrolyte	Catalyst (Substrate)	Catalyst Loading	Catalyst Mass	Cobalt Mass	Electrochemical Operation	Average Cobalt Leaching Percentage	Average Cobalt Leaching Rate	Reference
HER	1 M KOH	CoS_2 (Ti plate)	~2.1 mg/cm$^2_{geo}$	~4.2 mg	~1.9 mg$_{Co}$	-20 mA/cm$^2_{geo}$; 250 h	~59.4% (after 250 h) [2]	~0.24%/h (after 250 h)	ref. S20
HER	1 M KOH	Ce-doped CoS_2 (Ti plate)	~2.1 mg/cm$^2_{geo}$	~4.1 mg	~1.8 mg$_{Co}$	-20 mA/cm$^2_{geo}$; 250 h	~3.2% (after 250 h) [3]	~0.013%/h (after 250 h)	ref. S20
HER	0.5 M H_2SO_4	CoS_2/CNT (carbon fiber paper)	~0.8 mg/cm$^2_{geo}$	~0.4 mg	N/A	-0.077 V vs. RHE; 20 h	~17.5% (the initial 0.5 h) [2]	~35.0%/h (the initial 0.5 h)	ref. S21
							~6.7% (from 0.5 h to 20 h) [3]	~0.45%/h (from 0.5 h to 20 h)	
HER	0.5 M H_2SO_4	CoS|P/CNT (carbon fiber paper)	~0.8 mg/cm$^2_{geo}$	~0.4 mg	N/A	-0.077 V vs. RHE; 20 h	~5.0% (after 12 h) [3]	~0.42%/h (after 12 h)	ref. S21
OER	0.5 M H_2SO_4	300 nm Co_3O_4 film (FTO)	~0.36 mg/cm$^2_{geo}$ [3]	~0.36 mg [3]	~0.27 mg$_{Co}$ [3]	10 mA/cm$^2_{geo}$; ~10 h	~25% (after ~10 h) [3]	~2.5%/h (after ~10 h)	ref. S22
						1 mA/cm$^2_{geo}$; ~72 h	~34% (after ~72 h) [3]	~0.47%/h (after ~72 h)	
$2e^-$ ORR	0.05 M H_2SO_4	*o*-$CoSe_2$/CFP #2 (carbon fiber paper)	~1.4 mg/cm$^2_{geo}$	~1.4 mg	~0.37 mg$_{Co}$	0.5 V vs. RHE; 1.5 h + 2.5 h	~0.51% (the initial 1.5 h) [4]	~0.34%/h (the initial 1.5 h)	This work
							~0.07% (reused for 2.5 h) [4]	**~0.027%/h** (reused for 2.5 h)	

[1] "HER" stands for hydrogen evolution reaction, "OER" stands for oxygen evolution reaction.

[2] These values were present in the original literature.

[3] These values were calculated based on the information present in the original literature.

[4] These values were calculated based on the data of the *o*-$CoSe_2$/CFP #2 electrode presented in Fig. S22a.

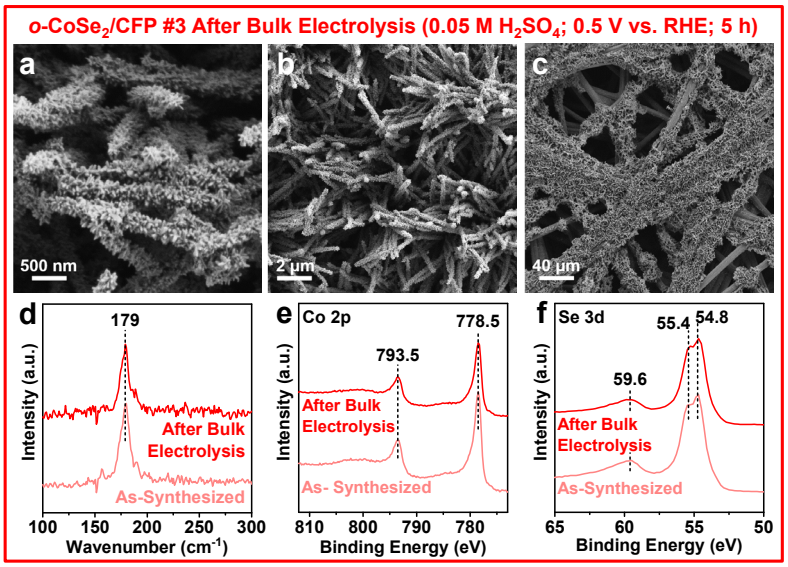

Fig. S23 (a–c) SEM images at different magnifications, (d) Raman spectra, (e) Co 2p and (f) Se 3d XPS spectra of the *o*-$CoSe_2$/CFP electrode #3 after the bulk electrolysis at 0.5 V vs. RHE in 0.05 M H_2SO_4 for 5 h (see Fig. S21). Background Raman spectra of bare carbon fiber paper substrate were subtracted from all as-measured Raman spectra of *o*-$CoSe_2$/CFP.

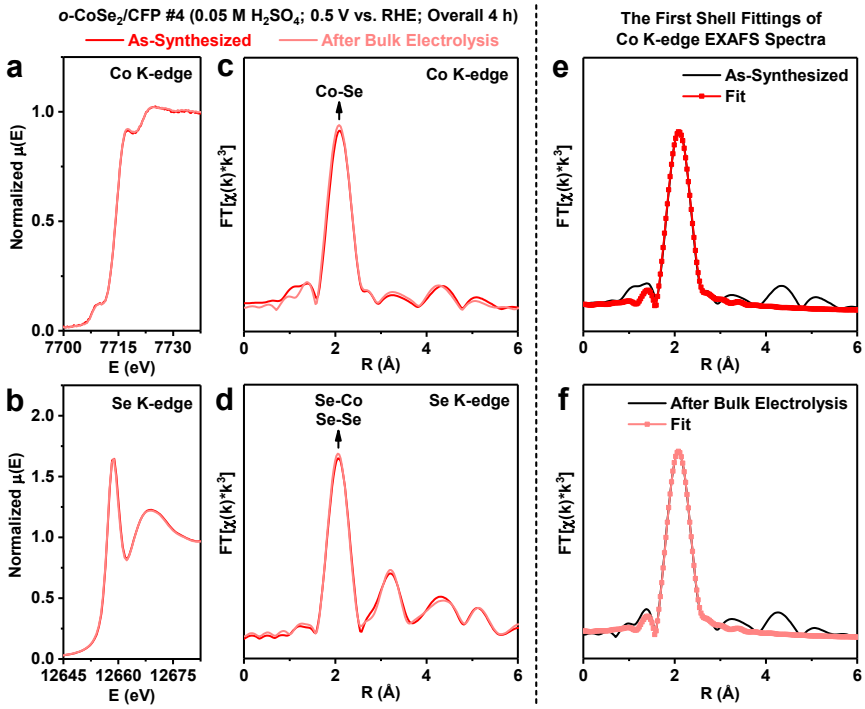

Fig. S24 (a) Co K-edge and (b) Se K-edge XANES spectra, Fourier transforms of (c) Co K-edge and (d) Se K-edge EXAFS spectra, and the first shell fittings of Co K-edge EXAFS spectra of the *o*-$CoSe_2$/CFP electrode #4 (e) before and (f) after the bulk electrolysis at 0.5 V vs. RHE in 0.05 M H_2SO_4 for overall 4 h (see Fig. S21). The Fourier transform parameters and fitting results are summarized in Table S15.

Table S15 The first shell fitting results of Co K-edge EXAFS spectra of the *o*-$CoSe_2$/CFP electrode #4 before and after the bulk electrolysis at 0.5 V vs. RHE in 0.05 M H_2SO_4 for overall 4 h.

Sample	Shell	N [b]	R (Å) [b]	σ^2 (10^{-3} Å^2) [b]	ΔE_0 (eV) [b]	Reduced χ^2 [b]	R-factor [b]
As-Synthesized	Co-Se	5.9 ± 1.1	2.411 ± 0.007	5.7 ± 0.7	1.9 ± 1.7	43.7445612	0.0120876
After Bulk Electrolysis	Co-Se	5.7 ± 1.0	2.405 ± 0.004	5.4 ± 0.4	0.9 ± 1.0	50.1007662	0.0042312

[a] For both samples, the Fourier transform parameters are: Hanning window, k_{min} = 3, k_{max} = 12, dk = 1, no phase correction; the fitting parameters are: r_{min} = 1, r_{max} = 3, dr = 0, fitting k-weight = 3.

[b] N is the coordination number of the absorbing Co atom. R is the interatomic distance between the absorbing Co atom and the backscattering S/Se atom. σ^2 is the mean square relative displacement (i.e., the Debye-Waller factor). ΔE_0 is the energy shift parameter used to align the theoretical calculated spectrum to the energy grid of the measured spectrum. For all the first shell fittings, the amplitude reduction factor (S_0^2) is constrained to 0.90 as a reasonable estimation, and the added uncertainty in the coordination number (N) due to the estimation of S_0^2 has already been considered.[S6] Reduced χ^2 and R-factor are goodness-of-fit parameters.

Table S16 Comparisons of the cumulative H_2O_2 concentrations achieved from bulk electrosynthesis of H_2O_2 in *acidic* solution using *o*-$CoSe_2$/CFP and other reported $2e^-$ ORR electrocatalysts in a similar H-cell setup. *See additional discussion on page S38.*

Classification	Catalyst	Catalyst Loading (Geometric Area)	*Acidic* Electrolyte (Volume)	Potential	Time	H_2O_2 Production Rate (mmol $g_{catalyst}^{-1}$ h^{-1})	Cumulative H_2O_2 Concentration	Cumulative H_2O_2 Selectivity	Catalyst Leaching Rate Monitored?	Reference
Earth-abundant transition metal compounds	*o*-$CoSe_2$/CFP	~370 $\mu g_{Co}/cm^2_{geo}$ ~1.42 $mg_{catalyst}/cm^2_{geo}$ (1 cm^2_{geo})	0.05 M H_2SO_4 (4 mL)	0.5 V vs. RHE	6 h	4.0	**547 ppm**	~70%	**Yes**	this work
Noble metal catalysts	Pt-Hg foil	N/A (0.98 cm^2_{geo})	0.1 M $HClO_4$ (15 mL)	0.4 V vs. RHE	~1 h	N/A	21 ppm	~80% [a]	No	ref. S7
Single-atom catalysts	Co_1-N-C(1)	100 $\mu g_{catalyst}/cm^2_{geo}$ (1 cm^2_{geo}) [b]	0.5 M H_2SO_4 (42 mL) [b]	0.5 V vs. RHE	4 h	9.7	3.1 ppm	~47% [a]	No	ref. S13
	Co_1-N-C(2)	100 $\mu g_{catalyst}/cm^2_{geo}$ (1 cm^2_{geo})	0.1 M $HClO_4$ (100 mL) [b]	0.5 V vs. RHE	10 h	80	27.2 ppm	~81%	No	ref. S14
	h-Pt_1-CuS_x	250 $\mu g_{catalyst}$ (3 cm^2_{geo})	0.5 M $HClO_4$ (110 mL) [b]	0.05 V vs. HOR [c]	1 h	546	~58 ppm	>90%	No	ref. S12
Carbon materials	meso-BMP	~307 $\mu g_{catalyst}/cm^2_{geo}$ (0.196 cm^2_{geo})	0.1 M $HClO_4$ (N/A)	0.1 V vs. RHE	4 h	N/A	13 ppm	N/A	No	ref. S18
	NCMK	50 $\mu g_{catalyst}/cm^2_{geo}$ (1 cm^2_{geo}) [b]	0.5 M H_2SO_4 (145 mL)	0.3 V vs. RHE	6 h	~35	~1.6 ppm	~87% [a]	No	ref. S19

[a] Cumulative H_2O_2 selectivity is calculated from the literature value of cumulative Faradaic efficiency using the following equation:

$$\text{Cumulative } H_2O_2 \text{ Selectivity } (\%) = 200 \times \frac{1}{1 + \frac{100}{\text{Cumulative Faradaic Efficiency } (\%)}}$$

[b] These information was not present in the original literature but was provided by the authors upon request.

[c] In this previous report,[S12] the authors operated the H-cell setup as a fuel cell, where the h-Pt_1-CuS_x catalyst was loaded on the cathode for H_2O_2 production and a Pt mesh was used as the anode for hydrogen oxidation reaction (HOR). The cell output was controlled at 0.05 V without any energy input. This operation mode was different from the rest of the previous reports in this Table S16, where the anode was used to drive water oxidation and the H-cell setup was operated as an electrolyzer.[S7, S13-S14, S18-S19]

Additional Discussion of Table S16 For on-site water treatment applications, it is essential to accumulate a practically useful H_2O_2 concentration up to 1000 ppm from bulk electrosynthesis.[S23] We demonstrated that *o*-$CoSe_2$/CFP successfully accumulated 547 ppm H_2O_2 over 6 h from the steady bulk electrosynthesis at 0.5 V vs. RHE in 0.05 M H_2SO_4 using a two-compartment three-electrode H-cell setup (Fig. 6 in the main text). We compare this cumulative H_2O_2 concentration achieved by *o*-$CoSe_2$/CFP with the few previous reports where the bulk electrosynthesis of H_2O_2 in *acidi*c solution was conducted on other $2e^-$ ORR electrocatalysts in a similar H-cell setup (Table S16). We found that these reported catalysts were operated in larger volumes of electrolyte solution, and the cumulative H_2O_2 concentrations were one or two order(s) of magnitude lower than 547 ppm (Table S16). Therefore, they were evaluated under much less stringent operating conditions because the catalyst stability was less challenged and the electrochemical side reactions of H_2O_2 reduction and/or decomposition were less probable to take place without a significant buildup of H_2O_2 concentration. Although the H_2O_2 production rate of *o*-$CoSe_2$/CFP (4.0 mmol $g_{catalyst}^{-1}$ h^{-1}, see Table S16) could be further improved by nanostructuring the catalyst and engineering the oxygen gas diffusion, *o*-$CoSe_2$/CFP shows enhanced catalyst stability and is highly resistant to electrochemical side reactions under stringent operating conditions, and the cumulative H_2O_2 concentration of 547 ppm is the highest among all the reported $2e^-$ ORR catalysts evaluated in *acidic* solution in a similar H-cell setup.

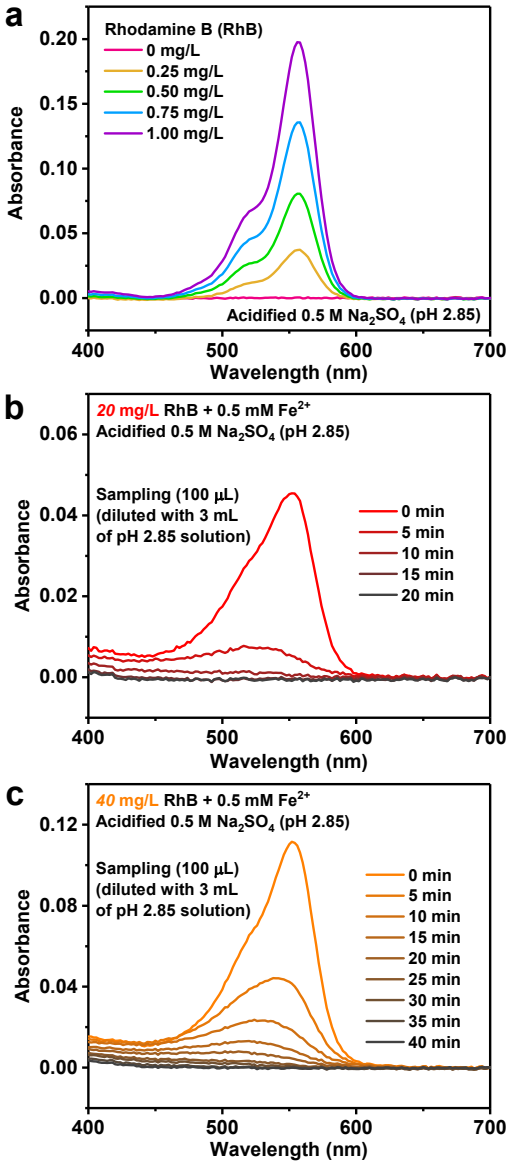

Fig. S25 (a) Absorption spectra of standard solutions of RhB (up to 1.00 mg/L) in acidified 0.5 M Na_2SO_4 solution (pH 2.85). (b,c) Absorption spectra of the quantitatively diluted small aliquot of electrolyte solution sampled from the working electrode compartment at various time points during each electro-Fenton degradation test shown in Fig. 7 in the main text: (b) 20 mg/L or (c) 40 mg/L RhB in O_2-saturated acidified 0.5 M Na_2SO_4 solution (pH 2.85) with the presence of 0.5 mM Fe^{2+}.

References Cited in the Electronic Supplementary Information

S1. The Materials Project, https://materialsproject.org/, (accessed April 14, 2020).

S2. W.-W. Zhao, P. Bothra, Z. Lu, Y. Li, L.-P. Mei, K. Liu, Z. Zhao, G. Chen, S. Back, S. Siahrostami, A. Kulkarni, J. K. Nørskov, M. Bajdich and Y. Cui, *ACS Appl. Energy Mater.*, 2019, **2**, 8605.

S3. A. K. Singh, L. Zhou, A. Shinde, S. K. Suram, J. H. Montoya, D. Winston, J. M. Gregoire and K. A. Persson, *Chem. Mater.*, 2017, **29**, 10159.

S4. H. Sheng, E. D. Hermes, X. Yang, D. Ying, A. N. Janes, W. Li, J. R. Schmidt and S. Jin, *ACS Catal.*, 2019, **9**, 8433.

S5. S. Grimme, J. Antony, S. Ehrlich and H. Krieg, *J. Chem. Phys.*, 2010, **132**, 154104.

S6. S. Calvin, XAFS for Everyone, CRC Press, 2013, pp. 353-354.

S7. S. Siahrostami, A. Verdaguer-Casadevall, M. Karamad, D. Deiana, P. Malacrida, B. Wickman, M. Escudero-Escribano, E. A. Paoli, R. Frydendal, T. W. Hansen, I. Chorkendorff, I. E. L. Stephens and J. Rossmeisl, *Nat. Mater.*, 2013, **12**, 1137.

S8. A. Verdaguer-Casadevall, D. Deiana, M. Karamad, S. Siahrostami, P. Malacrida, T. W. Hansen, J. Rossmeisl, I. Chorkendorff and I. E. L. Stephens, *Nano Lett.*, 2014, **14**, 1603.

S9. E. Pizzutilo, O. Kasian, C. H. Choi, S. Cherevko, G. J. Hutchings, K. J. J. Mayrhofer and S. J. Freakley, *Chem. Phys. Lett.*, 2017, **683**, 436.

S10. C. H. Choi, M. Kim, H. C. Kwon, S. J. Cho, S. Yun, H.-T. Kim, K. J. J. Mayrhofer, H. Kim and M. Choi, *Nat. Commun.*, 2016, **7**, 10922.

S11. S. Yang, J. Kim, Y. J. Tak, A. Soon and H. Lee, *Angew. Chem. Int. Ed.*, 2016, **55**, 2058.

S12. R. Shen, W. Chen, Q. Peng, S. Lu, L. Zheng, X. Cao, Y. Wang, W. Zhu, J. Zhang, Z. Zhuang, C. Chen, D. Wang and Y. Li, *Chem*, 2019, **5**, 2099.

S13. Y. Sun, L. Silvioli, N. R. Sahraie, W. Ju, J. Li, A. Zitolo, S. Li, A. Bagger, L. Arnarson, X. Wang, T. Moeller, D. Bernsmeier, J. Rossmeisl, F. Jaouen and P. Strasser, *J. Am. Chem. Soc.*, 2019, **141**, 12372.

S14. J. Gao, H. b. Yang, X. Huang, S.-F. Hung, W. Cai, C. Jia, S. Miao, H. M. Chen, X. Yang, Y. Huang, T. Zhang and B. Liu, *Chem*, 2020, **6**, 658.

S15. E. Jung, H. Shin, B.-H. Lee, V. Efremov, S. Lee, H. S. Lee, J. Kim, W. Hooch Antink, S. Park, K.-S. Lee, S.-P. Cho, J. S. Yoo, Y.-E. Sung and T. Hyeon, *Nat. Mater.*, 2020, **19**, 436.

S16. C. Tang, Y. Jiao, B. Shi, J.-N. Liu, Z. Xie, X. Chen, Q. Zhang and S.-Z. Qiao, *Angew. Chem. Int. Ed.*, 2020, **59**, 9171.

S17. Z. Lu, G. Chen, S. Siahrostami, Z. Chen, K. Liu, J. Xie, L. Liao, T. Wu, D. Lin, Y. Liu, T. F. Jaramillo, J. K. Nørskov and Y. Cui, *Nat. Catal.*, 2018, **1**, 156.

S18. F. Hasché, M. Oezaslan, P. Strasser and T.-P. Fellinger, *J. Energy Chem.*, 2016, **25**, 251.

S19. Y. Sun, I. Sinev, W. Ju, A. Bergmann, S. Dresp, S. Kühl, C. Spöri, H. Schmies, H. Wang, D. Bernsmeier, B. Paul, R. Schmack, R. Kraehnert, B. Roldan Cuenya and P. Strasser, *ACS Catal.*, 2018, **8**, 2844.

S20. J. Li, Z. Xia, M. Zhang, S. Zhang, J. Li, Y. Ma and Y. Qu, *J. Mater. Chem. A*, 2019, **7**, 17775.

S21. W. Liu, E. Hu, H. Jiang, Y. Xiang, Z. Weng, M. Li, Q. Fan, X. Yu, E. I. Altman and H. Wang, *Nat. Commun.*, 2016, **7**, 10771.

S22. J. S. Mondschein, J. F. Callejas, C. G. Read, J. Y. C. Chen, C. F. Holder, C. K. Badding and R. E. Schaak, *Chem. Mater.*, 2017, **29**, 950.

S23. S. Yang, A. Verdaguer-Casadevall, L. Arnarson, L. Silvioli, V. Čolić, R. Frydendal, J. Rossmeisl, I. Chorkendorff and I. E. L. Stephens, *ACS Catal.*, 2018, **8**, 4064.